# Numerical Solution of a 2-D Model for Formation of Zonal Jets

by

Girish Nigamanth Raghunathan

A Thesis Presented in Partial Fulfillment
of the Requirements for the Degree
Master of Science

Approved April 2017 by the
Graduate Supervisory Committee:

Huei-Ping Huang, Chair
Marcus Herrmann
Kangping Chen

ARIZONA STATE UNIVERSITY
May 2017

ABSTRACT

The formation and stability of a slowly evolving zonal jet in 2-D flow with beta effect is analyzed using the model developed by Manfroi and Young in which the final governing equation was derived by means of a perturbation analysis of a barotropic vorticity equation with sinusoidal meridional mean flow. However in the original study the term $\beta_0$, that represents the effect of large-scale Rossby waves, was dropped and was proceeded on a path of finding solutions for a simplified 1-D flow. The idea of this study is to understand the effects of the dropped term on the overall dynamics of the zonal jet evolution. For this purpose the system that is entirely deterministic with no additional forcing is solved by means of a standard finite difference scheme. The Numerical solutions are found for varying $\beta_0$ and $\mu$ values where $\mu$ represents the bottom drag. In addition to this the criteria for the formation of zonal jets developed originally for the 1-D system is verified for the 2-D system as well. The study reveals the similarity in some of the results of the 1-D and the 2-D system like the merging of jets in the absence of bottom drag, formation of steady jets in presence of a non-zero bottom drag and the adherence to the boundary criteria for the formation of zonal jets. But when it comes to the formation of steady jets, a finite $\beta_0$ value is required above which the solution is similar to the 1-D system. Also the jets formed under the presence of non-zero bottom drag seem wavy in nature which is different from the steady horizontal jets produced in the 1-D system.

ACKNOWLEDGEMENTS

I would like to express my utmost gratitude to Dr. Huei-Ping Huang for agreeing to guide me through the thesis work and for providing some valuable inputs on the topic guiding me throughout the process.

I also thank Dr. Herrmann and Dr. Chen for agreeing to be a part of my thesis committee.

TABLE OF CONTENTS

Page

CHAPTER Page

LIST OF FIGURES

Figure Page

Figure Page

Figure Page

Figure Page

# CHAPTER 1

## 1. INTRODUCTION:

Predicting atmospheric flows has been an important part in predicting the climate of a planet. One of the pivotal approaches used is the employment of two-dimensional turbulence models for doing so. It is known that at large Reynolds Number there is very little dissipation of energy and thus closely packed two dimensional eddies would propagate to larger scale unmitigated. However, Rhines in 1975 showed that this cascade towards large scales is halted as a result of existing background Rossby Waves which he indicated happens at a wave number of $k_b = \left(\frac{\beta}{2U}\right)^{\frac{1}{2}}$ where β is the vertical gradient of Coriolis component and U is the r.m.s. velocity of particle. He also suggested formation of anisotropic zonal mean flow as a result of the continuing cascade having a Jet Scale of $L_{rh} = \sqrt{\frac{U}{\beta}}$. [Rhines] Although the length scale of these jets has been accepted by several studies following this, the precise mechanism of the development of these anisotropic structures became the focal point of these studies. The problem studied in this research work is based on one such model developed to study the evolution of zonal jets.

### 1.1 Definitions

#### 1.1.1 Beta effect:

An important parameter when it comes to atmospheric dynamics and instabilities is the planetary beta effect. It arises as a direct consequence of varying planetary vorticity across the latitudes. This phenomenon is commonly noted in rotating

spheres and having a pronounced value when the speed with which the bodies rotate is higher. The formula for calculating $\beta$ is given below.

$$\beta = \frac{d\Omega}{dy}$$

Where Ω is the planetary vorticity at the latitude.

1.1.2 Rossby Waves:

Rossby Waves are oscillation produced about a latitude due to the instabilities perpendicular to the latitude in a horizontal air flow. The restoring force that makes it meander about the horizontal is a result of the planetary beta effect. These waves are also responsible for arresting the energy cascade in eddies to larger scales [Rhines 1975].

1.1.3 Zonal Jets:

Zonal Jets are anisotropic bands of alternating eastward and westward flows that form in several atmospheric as well as oceanic flows. These types of structures are seen in atmosphere of Jupiter (Figure 1.1). A striking feature of these structures is their persistence for a very long time and this coupled with discovery of their presence in atmosphere of several recently discovered large planets drove the motivation for studying their formation.

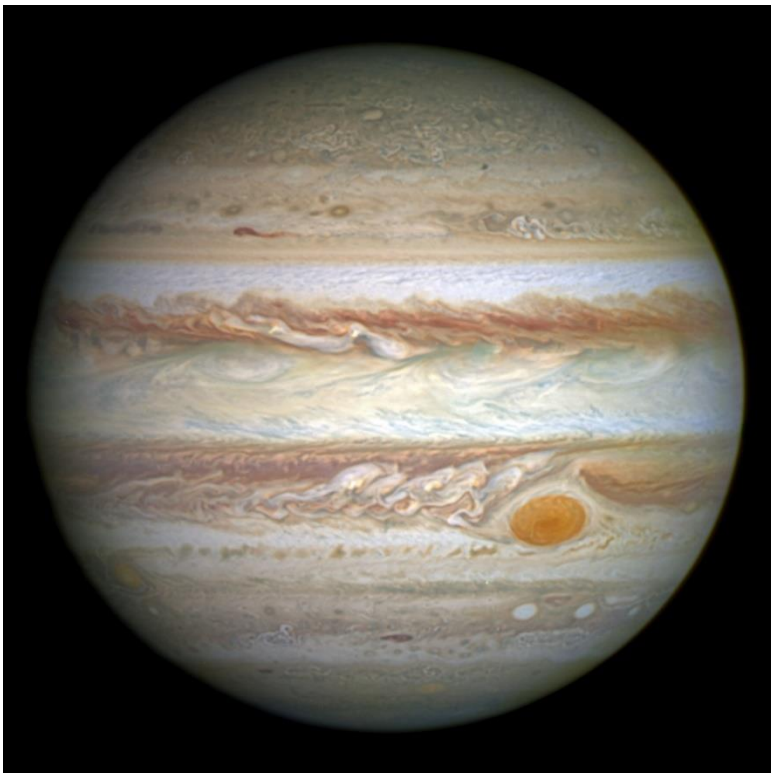

Figure 1.1 – Image showing the atmosphere of Jupiter (courtesy Wikipedia)

1.2 Literature Survey:

Following the paper by Rhines, Vallis and Maltrud in 1992 performed numerical simulations on a beta plane to produce zonal jets solving the vorticity equation directly for fixed value of β and a random small scale forcing term of varying wave number. The results confirmed the scaling relations by Rhines while producing intense and persistent zonal jets upon using a small-scale forcing. It was predicted that the formation of these persistent jets was a direct result of inverse energy cascade.

Huang and Robinson in 1998 performed the study in a rotating sphere analyzing the decay of turbulence in presence of zonal jets verifying the formula for anisotropic Rhines scale in process. Major prediction of this model was the reduced interaction of eddies closer to

Rhines scales with Zonal Jets suggesting that although the Rhines Scale barrier was valid for arrest of cascade to larger scale no evidence was seen for interaction of these eddies with zonal jets. There however was evidence of non-local energy transfer between the small-scale eddies and zonal jets which is thought to play the major role of maintaining the jets.

Noboru Nakamura and Da Zhu in 2009 suggested that the stirring due beta effect could produce a Potential Vorticity staircase which could be serve as a driving force for the zonal jets that are formed.

This idea was taken forward by R.S Scott and A.-S Tissier 2012 who then went on to suggest that jets can be formed also because of mixing of large scale waves which were previously thought to be discrete providing very less contribution to the development of jets.

1.3 Model Used:

The current study is performed based on the model by Manfroi and Young 1998 in which a small scale deterministic stirring is done on a base-state flow which when α=0 is nothing but a stationary Rossby wave. The starting point of the study is the vorticity equation

Vorticity equation

$$(\boldsymbol{\zeta} + \mathbf{f})_t + J(\psi, \boldsymbol{\zeta} + \mathbf{f}) = \mathbf{0} \qquad (\mathbf{1})$$

While in this case the planetary vorticity is taken as

$$\beta(sin\alpha x + cos\alpha y)$$

It is to be noted here that the vorticity equation ignores the divergence of velocity term based on the assumptions of incompressible flow. This assumption becomes questionable when it represents the system like Jupiter's atmosphere as the velocities reach close to sonic. However, this phenomenon of formation of zonal jets is not isolated to just this as we can also see them in Earth's Ocean where the velocities are much lesser and can be agreed to be incompressible. Also, given the large number of studies done based on the assumption of incompressible flow it is proceeded here based on the same assumption.

Also, the basic state flow was taken as

$$\left(\Psi, -\Psi_y, \Psi_x\right) = (-uy - \Psi_0 cosmx, u, m\Psi_0 sinmx)$$

Where $\Psi$ is Stream Function.

The total Stream Function is $\Psi(x, y) + \psi(x, y, t)$

Plugging this into the vorticity equation while non dimensionalizing the disturbance stream function as $\psi_{nondim} = \psi_{dim}/\nu$ the following equation is derived.

$$\nabla^2\psi_t + u\nabla^2\psi_x + Rsinx\left[\nabla^2\psi_y + \psi_y\right] + J(\psi, \nabla^2\psi) + \beta cos\alpha\psi_x - \beta sin\alpha\psi_y = \nabla^4\psi - \mu\nabla^2\psi \quad (2)$$

Following this a perturbation analysis is done for slightly supercritical Reynolds number

$$R = R_c(1 + \epsilon^2)$$

And several other variables are introduced based on multiscale expansion from several literature studies on the variables involved. The focus here is the result of this analysis which is the following equation and forms the starting point of our study.

$$A_{\eta\eta\tau} + 2A_{\eta\eta\eta\eta} + 3A_{\eta\eta\eta\eta\eta\eta} - \left[\left(\beta_1 - u_1 + A_\eta\right)^2 A_\eta\right]_{\eta\eta\eta} + \frac{1}{3}\left(A_\eta^3\right)_{\eta\eta\eta} + \beta_0 A_\xi - \alpha_5\beta_0 A_\eta$$

$$= -\mu_4 A_{\eta\eta} \qquad (3)$$

Where

$$A(\xi,\eta,\tau) = \psi_0, \quad \eta = \epsilon y, \quad \tau = \epsilon^4 t, \quad \mu = \epsilon^4\mu_4, \quad \alpha = \epsilon^5\alpha_5, \quad \xi = \epsilon^6 x$$

$\psi_0$→ Basic State Stream Function of the Disturbance.

$\xi, \eta$ → Non-Dimensionalized x and y coordinates.

$\tau$ → Non-Dimensionalized time.

$\mu_4$ → Non-Dimensionalized Bottom Drag term.

$\alpha_5$ → Non-Dimensionalized Angle of Inclination of Basic State Flow to the planetary vorticity.

$u_1$→Second term in the expansion of net advection term $u$.

$\beta_1$→Second term in the expansion of the term $\beta$.

$\epsilon$ → A small value controlling supercriticality of Reynold's Number.

$\beta$ and $u$ are expanded as

$$\beta = \beta_0 + \epsilon\beta_1 + \epsilon^2\beta_2 + \epsilon^3\beta_3 + \cdots$$

$$u = u_0 + \epsilon u_1 + \epsilon^2 u_2 + \epsilon^3 u_3 + \cdots$$

The equation **3** is derived upon collection of $\epsilon^6$ terms from the perturbation analysis. However, in this process the author had dropped the $\beta_0 A_\xi$ to make it a 1D system and had

done further analysis on this 1D system. It is seen that the dropped term represents the effect of large-scale Rossby waves. The objective of this research is to understand how the effect of large-scale Rossby waves affects the formation of zonal jets.

1.4 Plan of Research:

As a first step the simplified 1D system is first verified to ensure proper numerical scheme is used to solve the equation. The simplified 1D equation as given in the paper is

$$U_\tau = -\mu U - rU_{\eta\eta} - 3U_{\eta\eta\eta\eta} - 2\gamma(U^2)_{\eta\eta} + \frac{2}{3}(U^3)_{\eta\eta} \qquad (4)$$

Following this a numerical scheme is developed to solve the complete 2D system. The details of the numerical structure are discussed in the next chapter. The results of the simulation are found for various cases of $\beta_0$ and $\mu_4$. Comparison is done for specific results discussed in the paper and how it varies when it comes to the 2D model. Also, the results of the 2-D model are compared against the analytical $\mu$, $\gamma$ boundary derived to mark the arrest of zonal jet formation.

# CHAPTER 2

## 2. NUMERICAL SCHEME:

For coming up with a numerical solution a finite difference scheme is used which is 2nd order in space (a Central Difference Scheme) and 3rd order in Time (Runge-Kutta time integration method). It was essential to use a 3rd order Time stepping scheme as lower order integrations produced unstable solutions.

The domain length was 100 for the 1D system (as per the analysis by Manfroi and Young) and for the 2D system was taken as 100 * 100 in η and ξ directions.

### 2.1 Runge-Kutta Time Integration

For time integration, a Total Variation Diminishing (TVD) Runge-Kutta 3rd order scheme is used. The formula used for this purpose is given below.

For a generalized formula

$$\frac{\partial f}{\partial t} = F$$

Where,

F is the total spatially discretized right hand side of f at time level n.

f is the value of function at n+1 level. In this case f = $A_{\eta\eta}$.

$f^{(0)} = f^n$

$f^{(1)} = f^{(0)} + \alpha_{1,0}\, \Delta t\, F^{(0)}$

$$f^{(2)} = f^{(0)} + \alpha_{2,0}\,\Delta t\,F^{(0)} + \alpha_{2,1}\,\Delta t\,F^{(0)}$$

$$f^{(3)} = f^{(0)} + \alpha_{3,0}\,\Delta t\,F^{(0)} + \alpha_{3,1}\,\Delta t\,F^{(1)} + \alpha_{3,2}\,\Delta t\,F^{(2)}$$

$$f^{(3)} = f^{n+1}$$

For a TVD-RK3 Scheme

$$\alpha_{1,0} = 1, \alpha_{2,0} = -\frac{3}{4}, \alpha_{2,1} = \frac{1}{4}, \alpha_{3,0} = -\frac{1}{12}, \alpha_{3,1} = -\frac{1}{12}, \alpha_{3,2} = \frac{2}{3}$$

Ref: Lecture notes on Computational Fluid Dynamics by Dr. Herrmann.

2.2 Stable Time Step Size:

Now for taking a stable time step for a TVD RK-3 method we take the stability criteria for an FTCS.

$$\Delta t = CFL\frac{\Delta x}{max|a|}$$

Where a is maximum coefficient of hyperbolic term in the equation.

A simple expansion of the equation 3 and simplification would give the following equation.

$$A_{\eta\eta\tau} + 3A_{\eta\eta\eta\eta\eta\eta} - 4\gamma A_\eta A_{\eta\eta\eta\eta} - 12\gamma A_{\eta\eta\eta}A_{\eta\eta} - 2\left(A_\eta\right)^2 A_{\eta\eta\eta\eta} - 12A_\eta A_{\eta\eta}A_{\eta\eta\eta}$$
$$- 4\left(A_{\eta\eta}\right)^3 + (2-\gamma^2)A_{\eta\eta\eta\eta} + \beta_0 A_\xi - \alpha_5\beta_0 A_\eta = -\mu_4 A_{\eta\eta}$$

Thus, in this case the maximum coefficient of hyperbolic term would become $12\gamma A$ (since LHS is $A_{\eta\eta\tau}$). However, during the initial phase the value of A is very small thus a

minimum value of 0.01 is used. Thus, the stable time step used for this problem is as follows.

$$\Delta t = min\left(0.8\frac{\Delta x}{max|12\gamma A|}, 0.01\right)$$

2.3 Meshing Type

A uniform face centered mesh is used for this problem with a total of 141 nodal points (extra 6 points to accommodate for boundary on each side as a sixth order differential term is used). The domain length of 100 is divided into 128 elements.

An important reason why the choice of 128 elements would suffice in replicating the true behavior of the system hinges on the fact that when it comes to 2D turbulence in atmospheric flows the energy cascade always proceed in a direction from small scale to large scales. Given this the possibility of breakage in solution due to the limit in grid size is avoided. However, this may give rise to a different problem of piling energy into the large scale because of lack of diffusion of energy at such large scales. Thus, for the current choice though most of the results would carry the essence the original set of equations, there would be results (concerning merging of jets while there is no bottom drag) when a finer mesh would provide better results. But given such finer meshes would take much more time (4 times) for simulation given the corresponding reduction in time step size based on stability it was found 128 elements would be a more optimum value for the analysis.

2.4 Initial Condition:

The initial condition used is a random variable declared in both x and y direction to avoid presence of any preexisting bias for formation of coherent structures.

2.5 Boundary Condition:

The problem is defined in a periodic domain along x and y axes. Thus, a periodic boundary condition is used along both these axes. In addition to this the summation of stream function along y is taken as 0 at each time step as there is no net momentum in x direction as defined by the problem.

2.6 Finding A from $A_{\eta\eta}$:

A matrix is formed out of second derivative finite difference formula employing boundary conditions for first and last rows. Since 128 nodes are used a 128*128 matrix is defined. In case of using more nodes a more efficient way would be to use a V-Cycle. However, in this case given the simplicity of the matrix and since the matrix is formed and inverted only once it is easier to use this method. Also, it is noted that using the boundary conditions directly into the matrix makes it a singular matrix. Thus, the last row of the matrix is replaced with the condition that stream function along y direction add up to give zero.

# CHAPTER 3

## 3. RESULTS AND DISCUSSION:

Results of solving the 2D equation was found with the value of stream function field found at the end of the time interval. The primary plots that were used for comparison were the Harmon Diagram showing the evolution of zonal mean of horizontal velocity with time. Also, a contour plot of stream function at the end of the time interval is shown. The results were found by varying the parameter $\beta_0$ and bottom drag $\mu_4$ mainly to study the effect of those parameters on the formation of zonal jets. The results are found for two cases, one with the case where the basic state forcing is along a plane inclined to axis of rotation ($\alpha$=1) and other with case of basic state forcing parallel to axis of rotation ($\alpha$=0). First section will have a brief discussion on the numerical solution for 1D model using a random initial condition

### 3.1 Numerical Solution for the simplified 1D system:

In case of the 1D system the Horizontal velocity field is found at the end of $\tau$=2000 based on the formula 4. The evolution of jets and the merging is captured by the Harmon Diagram shown in Figure 3.1. Figure shows the evolution of jet for increasing cases of bottom drag $\mu$. Though the initial conditions used are different the ones used in Manfroi and Young one can see similar characteristics being maintained from the figures. Also, it is to be noted that since this is a 1D system it assumes of uniformity in Horizontal Velocity along the x direction.

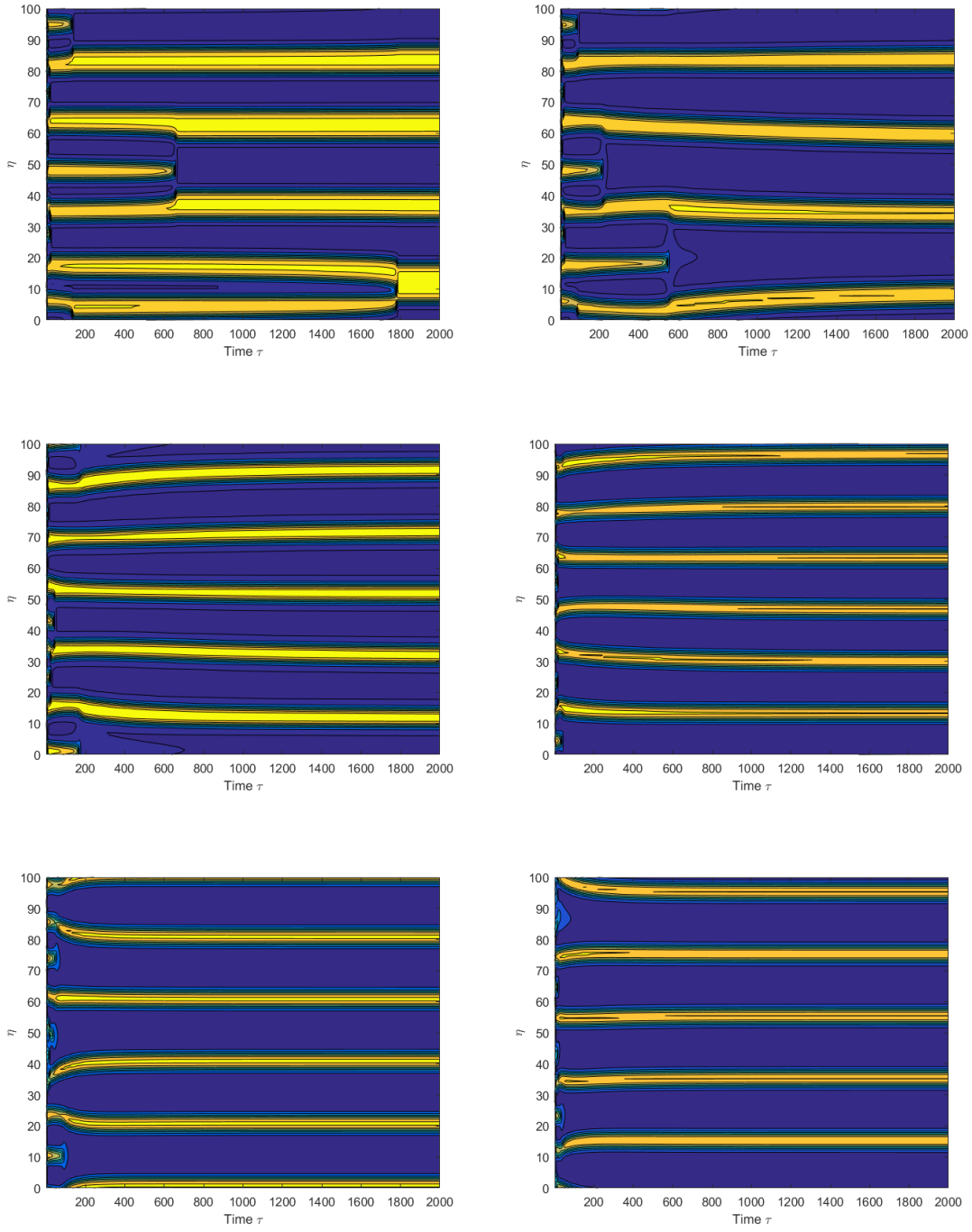


Figure 3.1 Contour Plot Showing Variation of Zonal Mean with Time Scale τ for Values of μ = 0, 0.01, 0.02, 0.05, 0.07, 0.09

3.2 Case of Parallel Basic State Forcing (α=0):

Since the angle α=0, the value of β would be constant at each point which is the case in most of the atmospheric flows. We will first see the results for case with no bottom drag.

3.2.1 Case with no bottom drag (μ=0):

Figure 3.3 shows the Harmon Diagram for cases of increasing $\beta_0$ value with no bottom drag. Figure 3.4 shows the Stream Function plot at the end of the time integration for those cases.

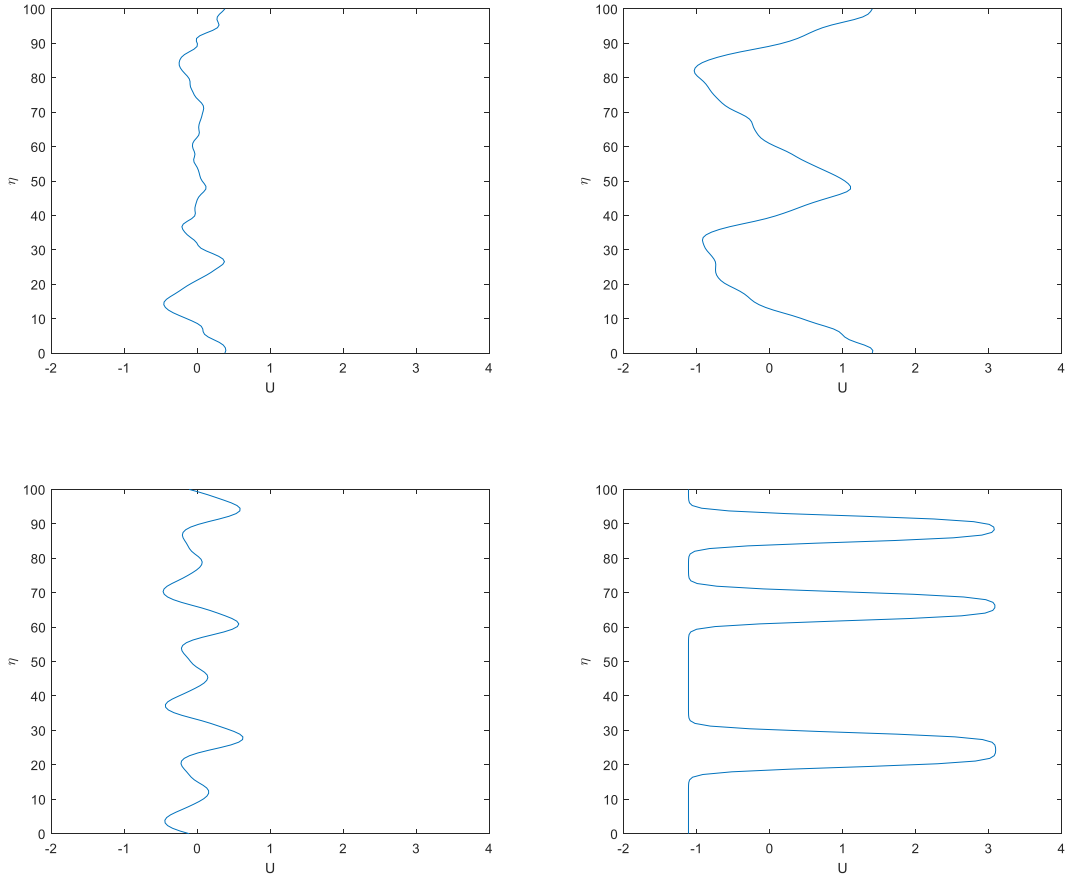


Figure 3.2: Line Plot of Zonal Mean at the End of τ=2000 α=0 $\beta_0$ = 0, 0.001, 0.01, and 0.1.

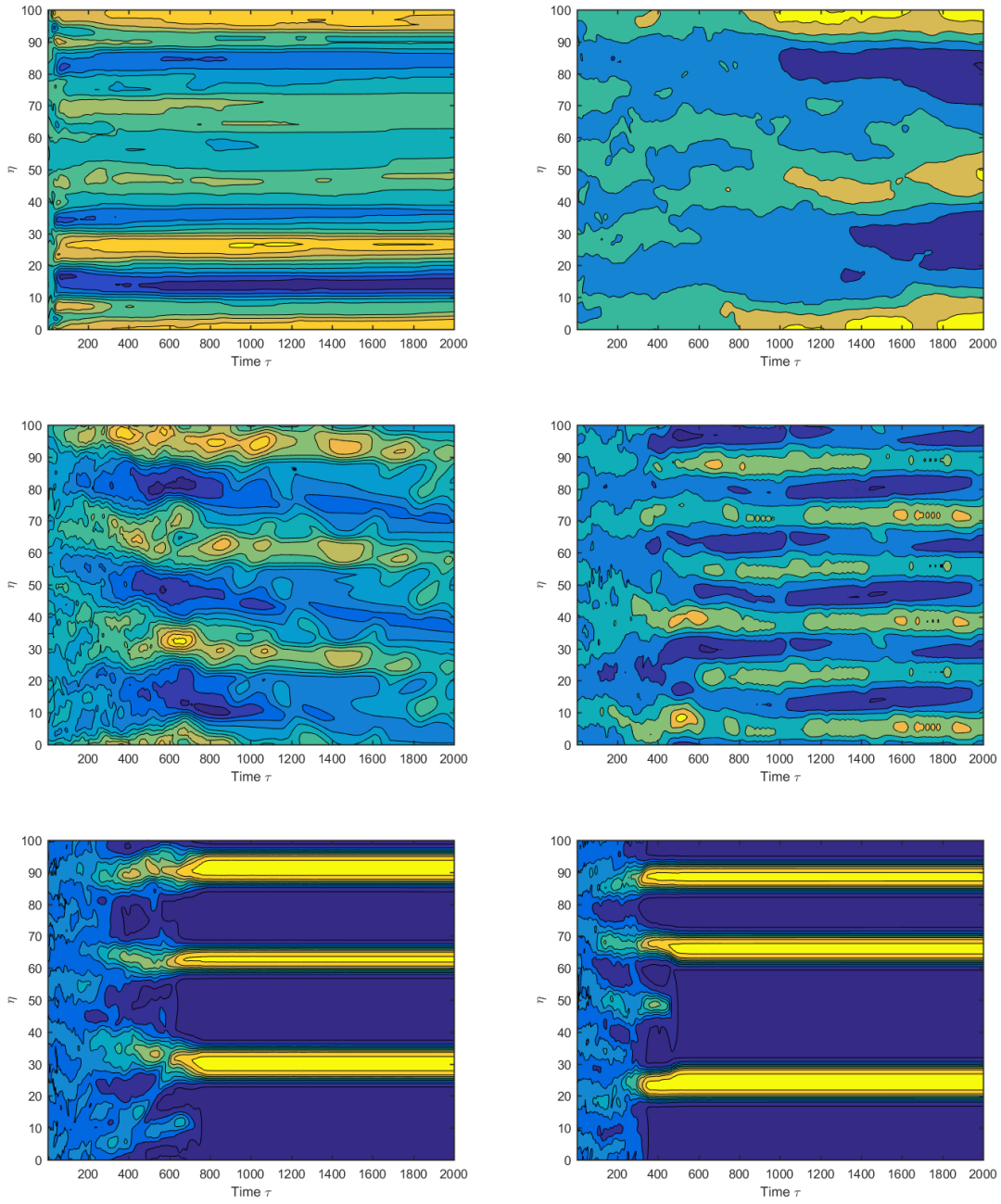


Figure 3.3: Contour Plot Showing Variation of Zonal Mean with Time Scale τ for Values of $\beta_0$ = 0, 0.001, 0.005, 0.01, 0.05, 0.1 from Top Left to Bottom Right Respectively for Case with No Bottom Drag ($\mu_4$ = 0)

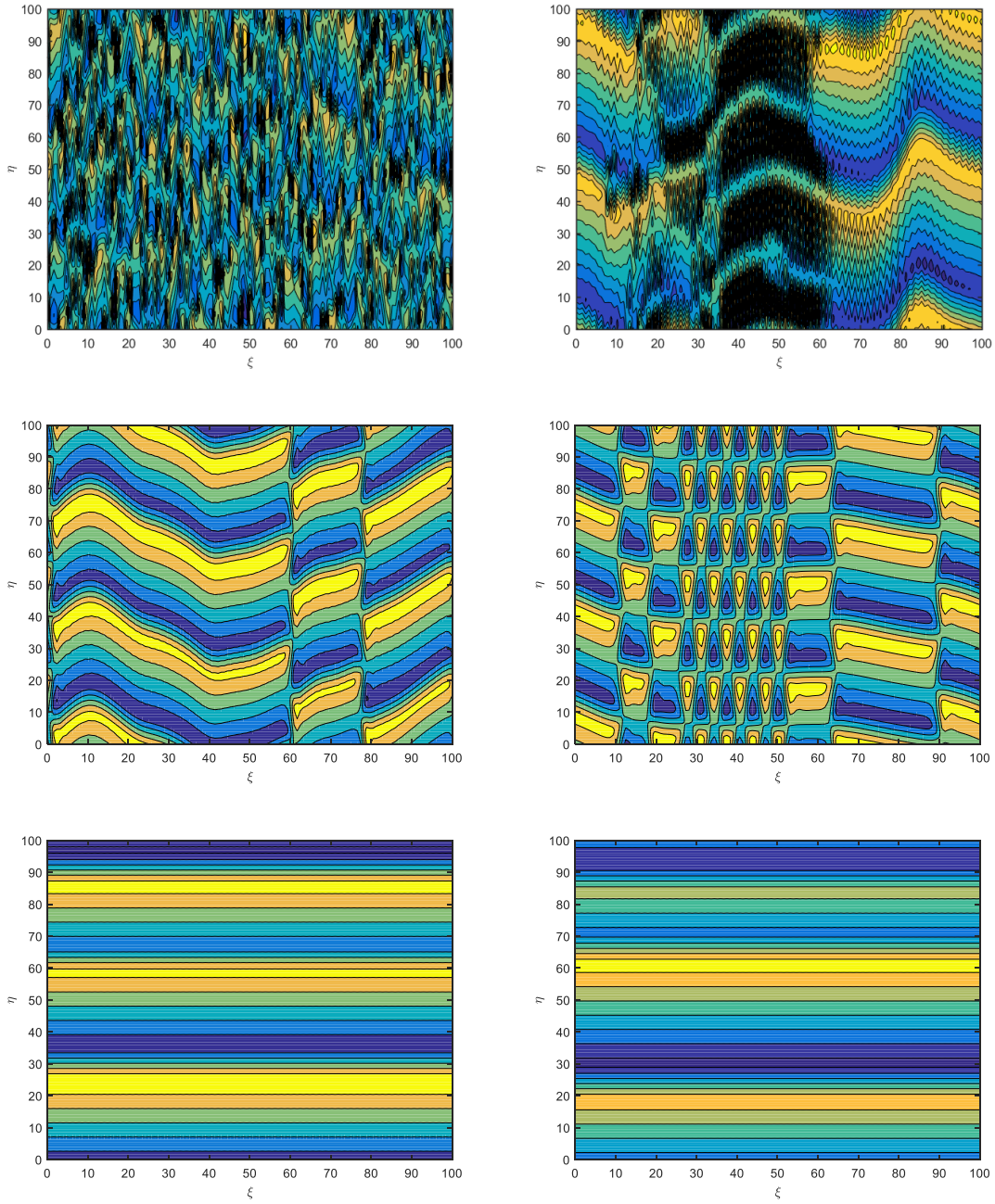


Figure 3.4 Contour Plots Showing Stream Function as a Function of ξ and η Versus the Coordinates ξ and η for Values of $\beta_0$ = 0, 0.001, 0.005, 0.01, 0.05, 0.1 from Top Left to Bottom Right Respectively for the Case with No Bottom Drag ($\mu_4$ = 0) at Time τ=2000.

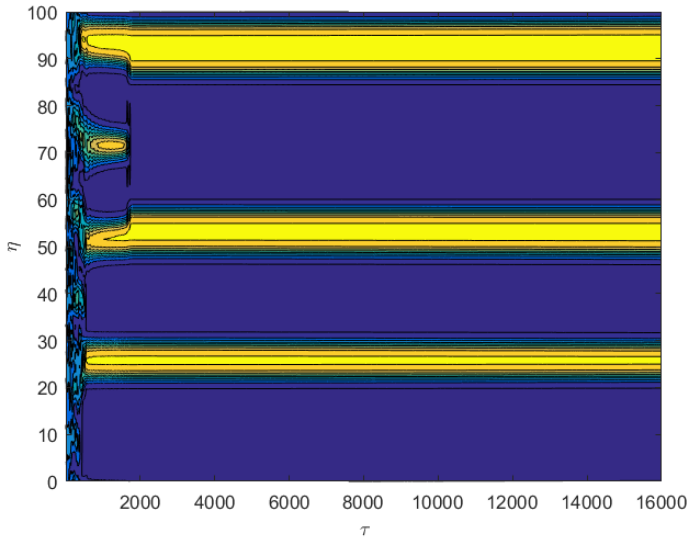


Figure 3.5 Contour Plot Showing Variation of Zonal Mean with Time τ for $\beta_0 = 0.1$.

3.2.2 Case with finite Bottom Drag ($\mu \neq 0$)

The figures 3.6, 3.7 show selected Harmon Diagram for cases of increasing bottom drag which is varied from 0.01 all the way till 0.087 the point at which zonal jets are no longer created. There are also figures showing stream function at the end of the time step for these case following which there is a plot summarizing all the runs spanning the $\beta_0$ and $\mu$ space denoting the number of jets in each of those cases.

3.2.3 Discussion on the results:

The term $\beta_0$ here represents in a way the gradient in potential vorticity. However, from the perturbation analysis done by Manfroi and Young it was seen that this is synonymous with net planetary advection. It could be seen from the results that this plays a major role in the formation of jets with greater value of $\beta_0$ (above 0.05) showing more pronounced zonal flow. A plot of zonal mean at the end of time integration for these cases show that the

intensity of the anisotropic zonal velocity match that of the 1D system. However, the cases with lesser $\beta_0$ show flows with reduced mean velocity. Another observation from these results is the number of evolving jets. Although a random initial condition is used in every one of the runs, we can see that for case with no bottom drag the number of jets evolving is always three. This also is in close correlation with the 1D case where 4 jets where seen.

Another important prediction of Manfroi and Young is the continuous merging of these formed jets until only 1 jet is left. However, there is no evidence of merging seen among the cases when integrated till $\tau$=2000. To confirm this fact simulations were performed taking one of the cases and running them till $\tau$=16000 whose result is shown in figure 3.5. It can be seen that the same three jets remained unmerged for up to $\tau$=16000. Part of a reason for this is the large separation between the sharp easterly jets which thereby may take a very long time to merge. However, since the system reverts to and can be compared with uniform 1D system, it is assumed that the property holds for the 2D system too. Also in the case where $\tau$=16000 one can see the merging occurring at around 2000 bringing the jets down from 4 to 3. This in addition to the fact that for the 1D case at the end of $\tau$=2000 there were 4 jets can be taken as an evidence of jet merging.

The crucial effect of adding bottom drag is the gradual thinning of jet scale because of the increasing bottom drag as reported in Manfroi and Young. This can be seen through the series of plots from 3.6 till 3.9. As a result of this the number of jets rise from 3 in the case with no bottom drag to almost 6 for the case where $\mu_4$=0.086 which is just before the jets disappear when $\mu_4$=0.087.

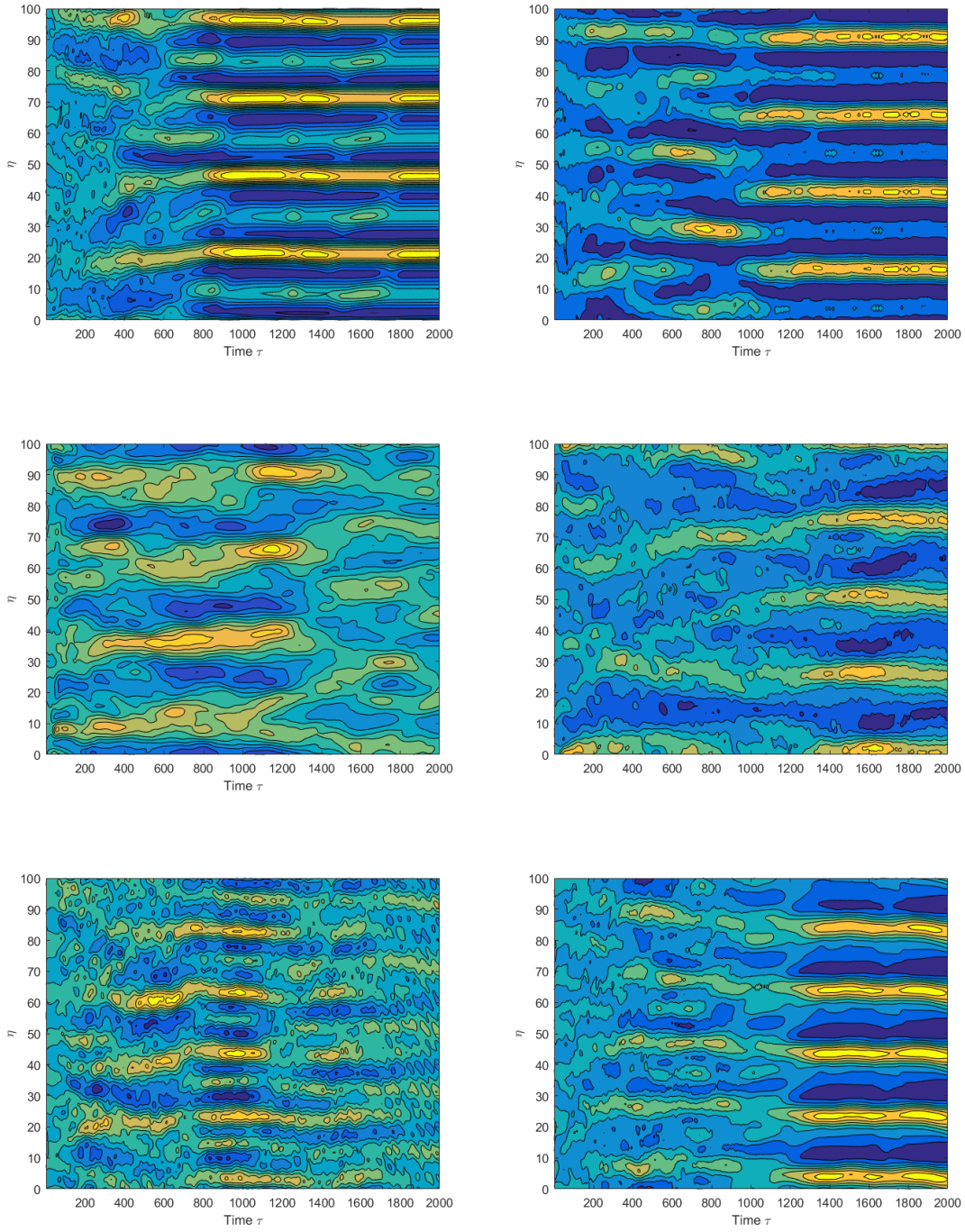


Figure 3.6 Contour Plot Showing Variation of Zonal Mean with Time Scale τ for Values of ($\beta_0$, $\mu_4$) = (0.01, 0.01), (0.03, 0.01), (0.001, 0.02), (0.004, 0.02), (0.006, 0.05), (0.01, 0.05) from Top Left to Bottom Right Respectively.

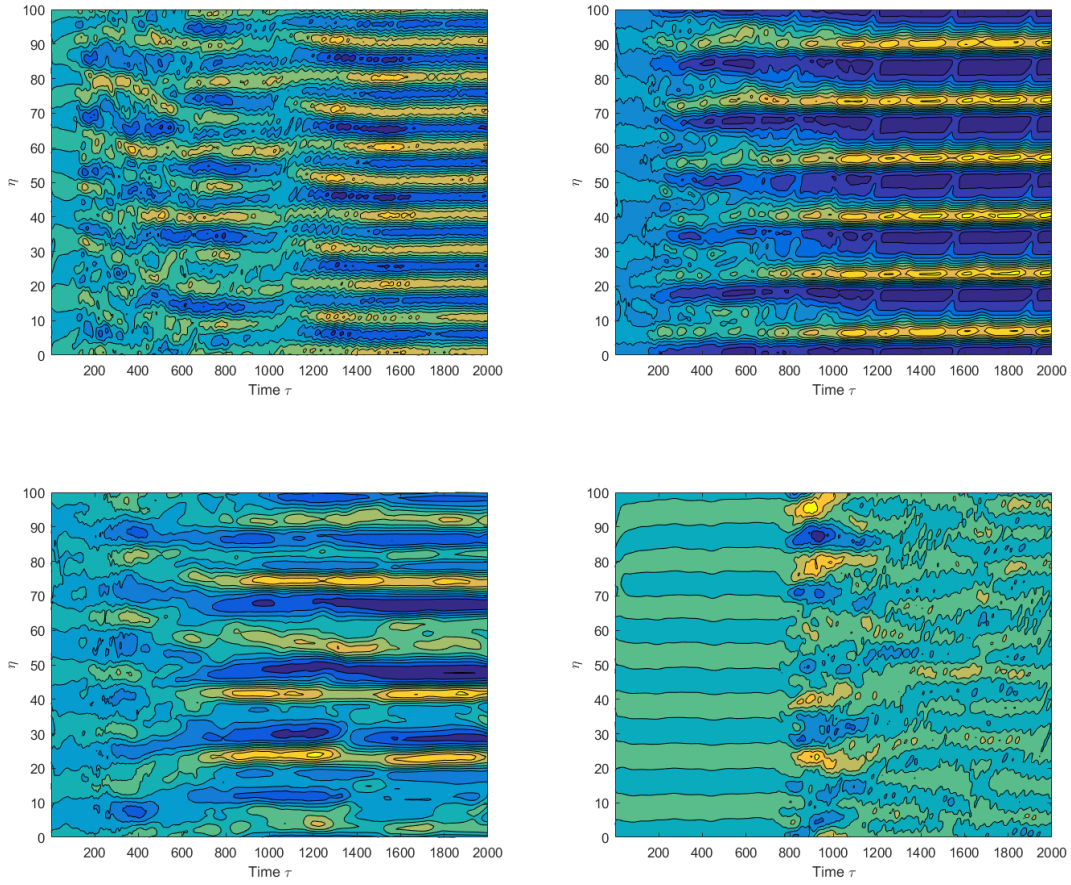


Figure 3.7 Contour Plot Showing Variation of Zonal Mean with Time Scale τ for Values of ($\beta_0$, $\mu_4$) = (0.01, 0.07), (0.05, 0.07), (0.02, 0.075), (0.01, 0.086) from Top Left to Bottom Right Respectively.

The value of $\beta_0$ above which the wavy as well as zonal jets are formed varies for different values of bottom drag and increases as the bottom drag increases. For example, from the plots we can see that for $\mu_4 = 0.05$ a value of $\beta_0 = 0.01$ produces a continuous wavy jet whereas as $\mu_4$ is increased to 0.07 this occurs at $\beta_0 = 0.02$.

Another important feature of these cases is the persistent wavy jets like the one seen in Figure 3.8. Though the reason is unknown this is thought to be the effect of background large scale rossby wave as such structures are seen as an effect of having a finite $\beta_0$ value and as this value is increased further the waviness decreases and zonal flows become pronounced. This is demonstrated in the later section.

A possible explanation is in presence of a large $\beta_0$ there is a huge driving force that can nullify the effect of bottom friction defeating any tendency of the jet stick to wavy form. This could be seen from the fact that when the bottom drag value is less we see much lesser meridional excursions. Also, this would explain the requirement of a larger $\beta_0$ for maintaining a continuous wavy jet as the bottom drag value increases.

These wavy structures once formed continues to move unaltered for a very long time like the zonal jets. Also, the intensity of Eastward and Westward jets at individual $\xi$ coordinate are the same as the 1D approximation of this system.

Another interesting feature that can be seen in case of small bottom drag but a finite value of $\beta_0$ is the presence of many number of large scale eddies. One can recall from the discussion in Huang and Robinson that the eddies that reach the Rhines scale do not contribute to the persistence of jets and thereby remain discrete. The feature found in Figure 3.8 is thought to be a depiction of this effect. The reason this happens is because in the initial phase of evolution when most of the energy is concentrated in the small scales and since a random initial condition is used the energy concentration in non-uniform. Thus if due to cascade large scale eddies get created they continue to persist along with the zonal jets contributing very little to persist the jets.

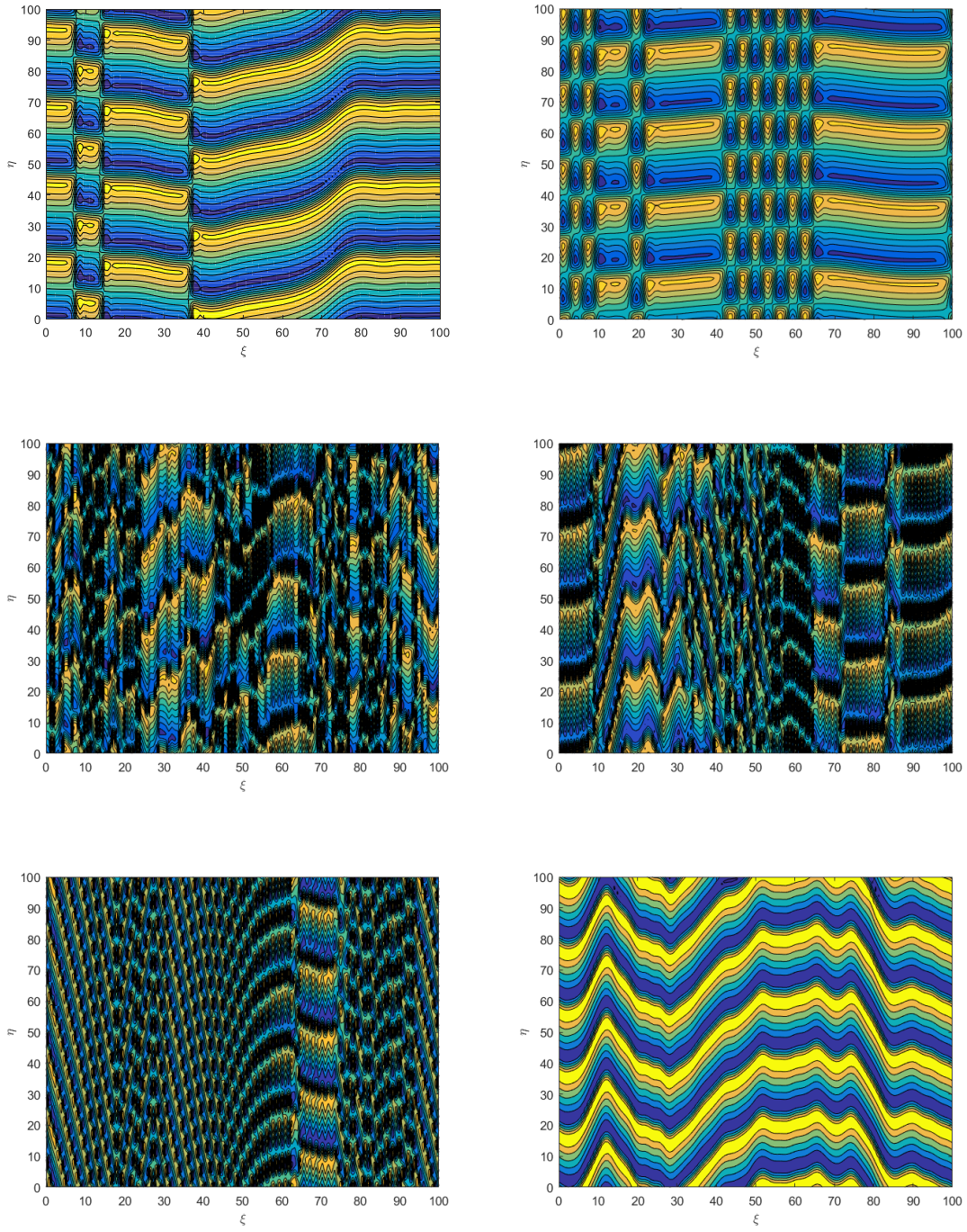


Figure 3.8 Contour Plot Showing Stream Function as a Function of ξ and η Versus the Coordinates ξ and η for Values of ($\beta_0$, $\mu_4$) = (0.01, 0.01), (0.03, 0.01), (0.001, 0.02), (0.004, 0.02), (0.006, 0.05), (0.01, 0.05) from Top Left to Bottom Right Respectively at Time τ=2000.

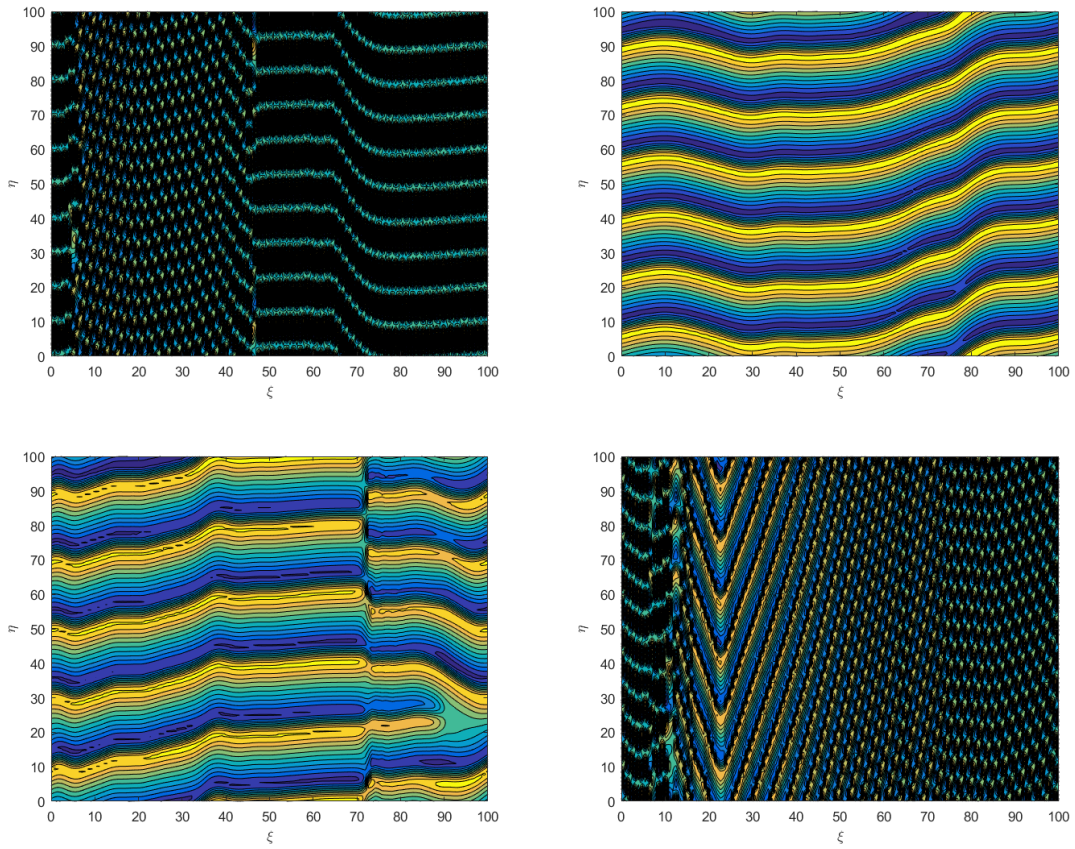


Figure 3.9 Contour Plot Showing Stream Function as a Function of ξ and η Versus the Coordinates ξ and η for Values of ($\beta_0$, $\mu_4$) = (0.01, 0.07), (0.05, 0.07), (0.02, 0.075), (0.01, 0.086) from Top Left to Bottom Right Respectively at Time τ=2000.

### 3.3 Case of Inclined Basic State Forcing ($\alpha$=1):

When the parameter $\alpha$ is varied setting it to a value of 1, the problem becomes a case where there is a vertical north south stirring along with an inclined basic state forcing. This type of problem gives rise to some interesting jet structures with migration of these structures towards the poles at a rate that is determined by the value of $\beta_0$.

We analyze cases like ones analyzed in the first case (With parallel basic state forcing). Also, there will be some discussion on jet structure and effect on bottom friction $\mu$ and $\beta_0$ on the same.

#### 3.3.1 Case with no bottom drag ($\mu$=0):

The Figures 3.10 and 3.11 show that with increasing value of $\beta_0$ the rate at which migration occurs towards the pole varies. Also for the case with no bottom drag we can see that the zonal jets are elongated not meridionally but along the direction of the basic state forcing. This happens for a value of $\beta_0$ greater than 0.002 as seen from the plot of stream function at the end of $\tau$=2000.

#### 3.3.2 Case with finite bottom drag ($\mu \neq 0$):

Similar to the case with parallel basic state flow the Figures 3.12 to 3.14 show the Harmon Diagram for various values of $\beta_0$ and increasing $\mu_4$ from 0.01 to 0.087. It is to be noted that despite having an inclined basic state flow the seizure of zonal jet formation occurs at the same value of 0.087 as the case with parallel basic state flow.

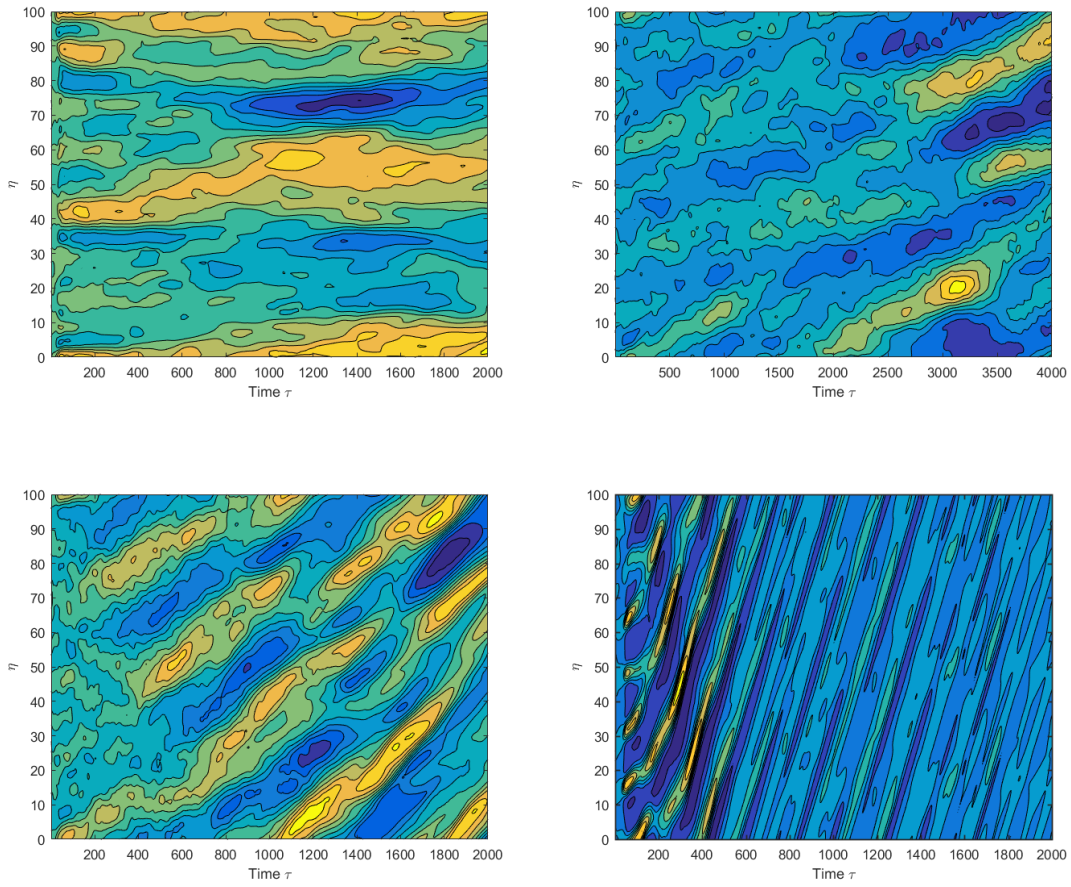


Figure 3.10 Contour Plot Showing Variation of Zonal Mean with Time Scale τ for Values of $\beta_0$ = 0, 0.0001, 0.001, 0.002, 0.01 from Top Left to Bottom Right Respectively for Case with No Bottom Drag ($\mu_4$ = 0) and α=1

3.3.3 Discussion on the Results:

One can see that changing the case from a parallel to an inclined basic state forcing affects the Harmon Diagram in that we see a slow migration of the jets towards the north. Also one can see that for the case with no bottom drag the jet tend to incline themselves in the direction of the basic state forcing as the value of $\beta_0$ is increased (in this case over a value of 0.002).

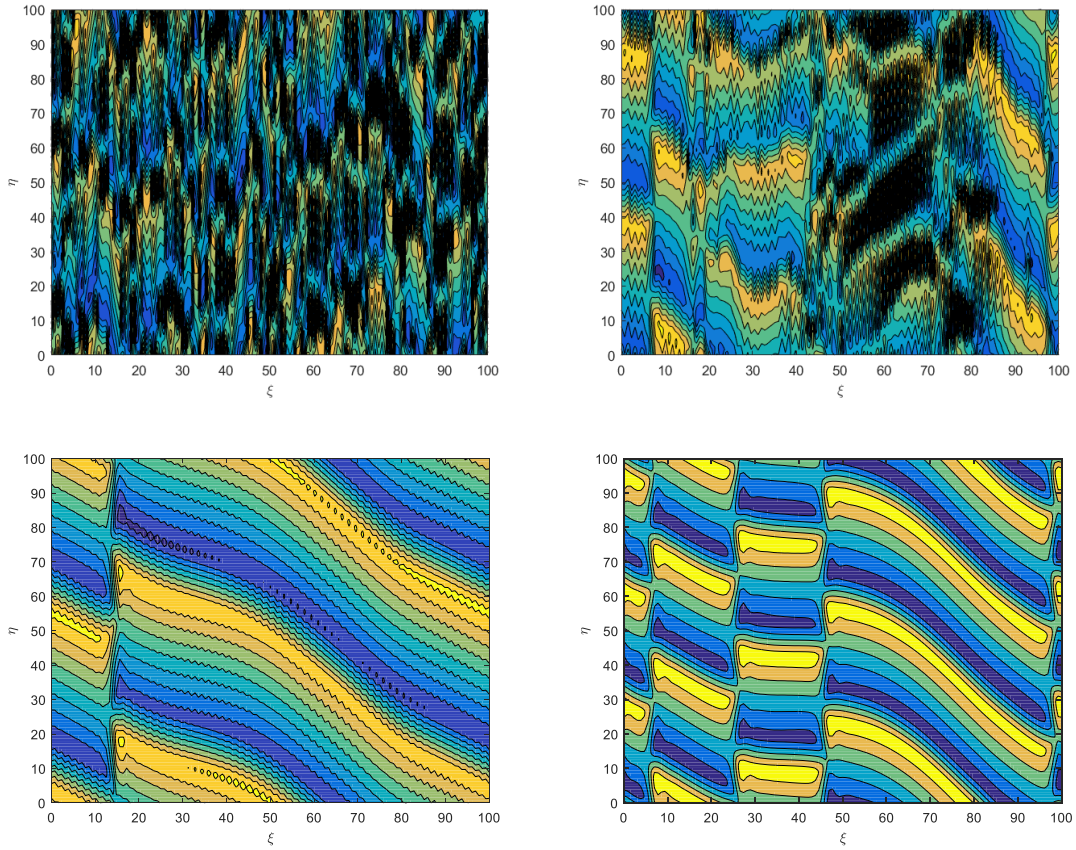


Figure 3.11 Contour Plot Showing Stream Function at $\tau$=2000 for Values of $\beta_0$ = 0, 0.0001, 0.001, 0.002, 0.01 from Top Left to Bottom Right Respectively for Case with No Bottom Drag ($\mu_4$ = 0) and $\alpha$=1

Also, like the first case, there was no conclusive evidence to suggest the merging of the jets in the absence of bottom drag. In the first case, however we could see system revert itself back to the uniform 1D type zonal jet and it was argued though merging wasn't seen explicitly it would occur upon continuous integration for a long time. But in this case since there is a constant migration and because the jets seem to be inclined the same argument cannot be made.

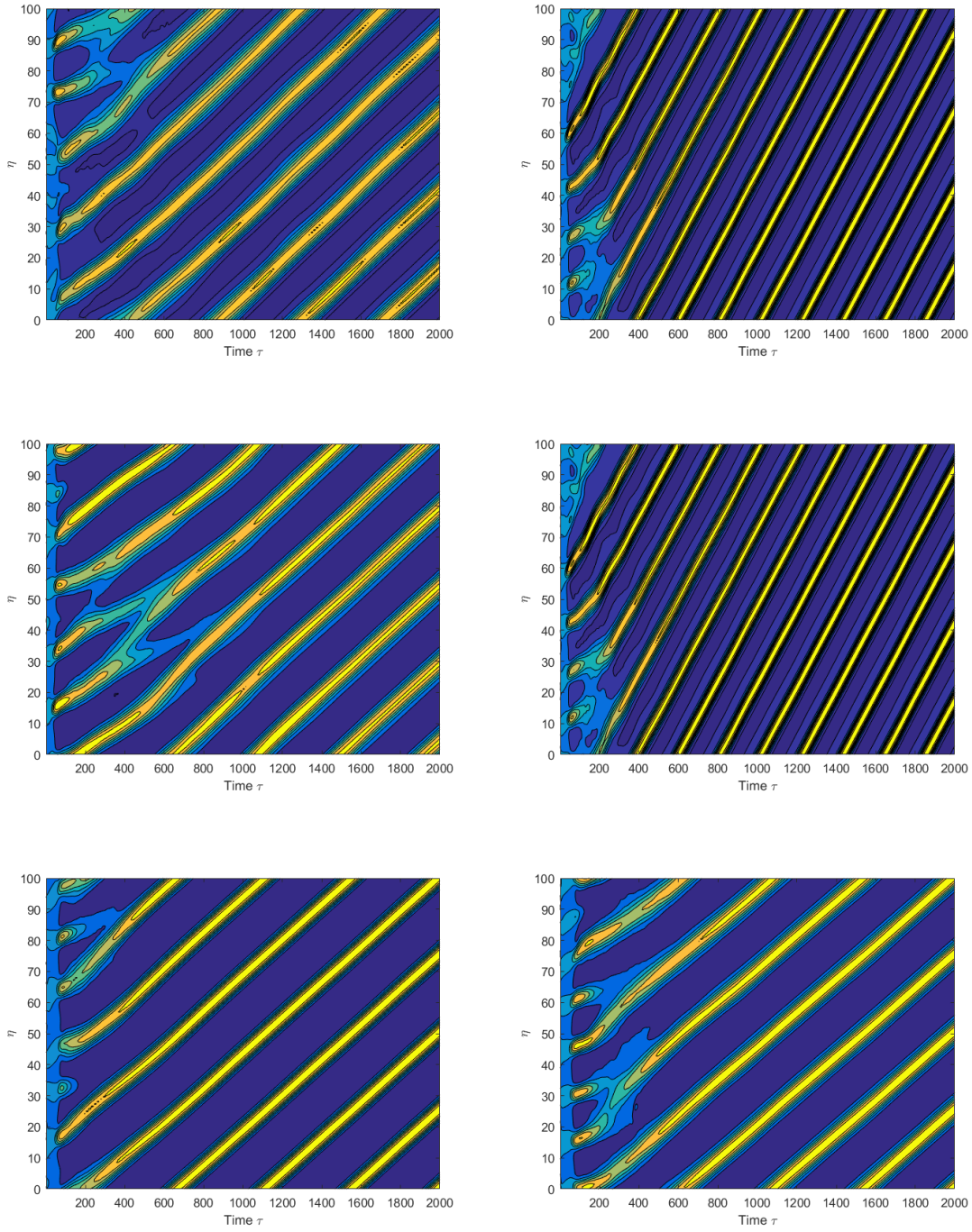


Figure 3.12 Contour Plot Showing Variation of Zonal Mean with Time Scale τ for Values of ($\beta_0$, $\mu_4$) = (0.005, 0.01), (0.01, 0.01), (0.005, 0.02), (0.01, 0.02), (0.005, 0.03), (0.005, 0.04) from Top Left to Bottom Right Respectively for α=1.

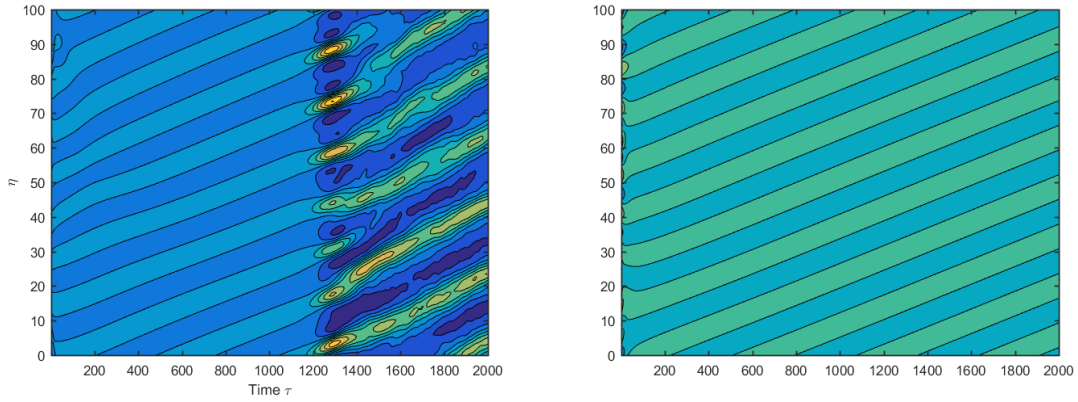


Figure 3.13 Contour Plot Showing Variation of Zonal Mean with Time Scale τ for Values of ($\beta_0$, $\mu_4$) = (0.005, 0.085), (0.005, 0.087) for α=1.

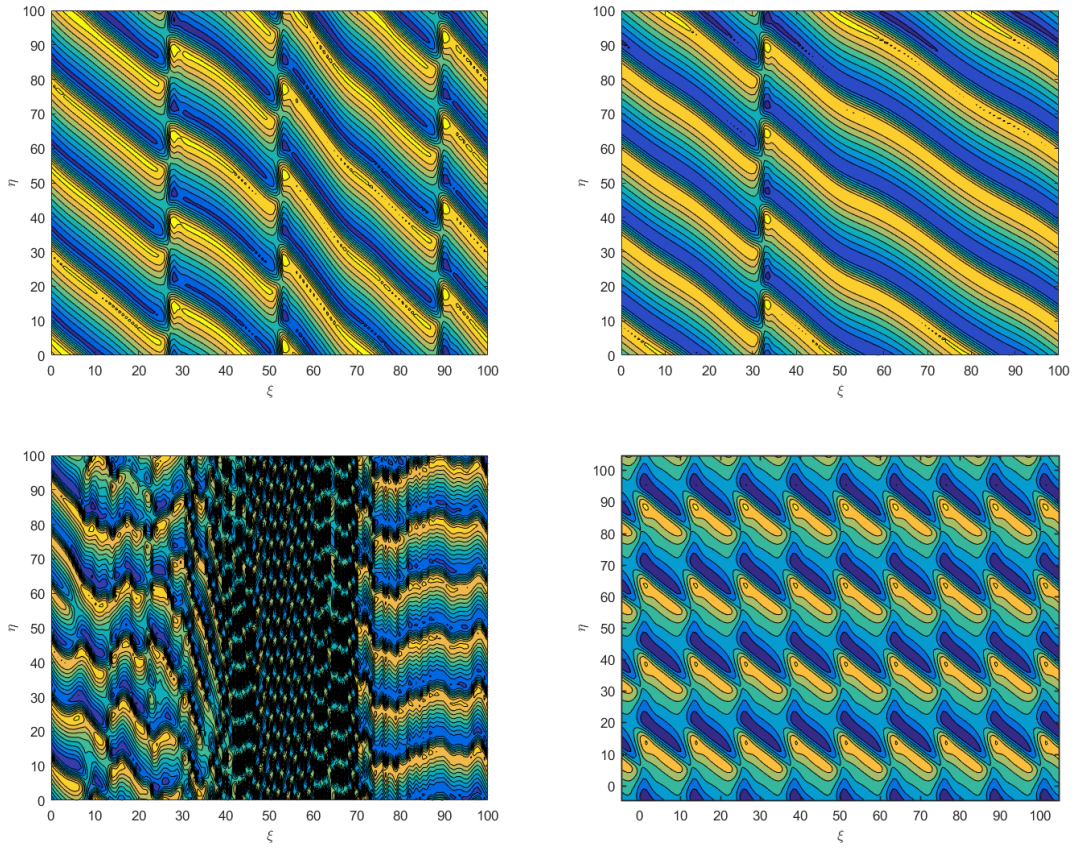


Figure 3.14: Contour Plot Showing Stream Function as a Function of ξ and η Versus the Coordinates ξ and η for Values of ($\beta_0$, $\mu_4$) = (0.0156, 0.01), (0.0156, 0.02), (0.0156, 0.08), (0.05, 0.086) from Top Left to Bottom Right Respectively at Time τ=2000.

3.4 Formation and Stability of Zonal Jets with varying γ:

The problem of stability of zonal jets was studied by Manfroi and Young suggesting through an analytical study that this happens when the viscosity is below as certain critical value $\mu_c$ and this varies as a function of γ which is the effective planetary vorticity gradient ($\gamma = \beta_1 - u_1$). It is further suggested in their study that despite having this limit, the solutions from the 1D system did not seem to follow the limit for certain cases. For example, as it can be seen from Figure 3.15, though the limiting viscosity value for case with γ=1 was 0.0833 we could still see jet formation at $\mu_4$=0.1. It can be seen from figures 3.17 and 3.18 that better adherence to this limit can be seen when it comes to the 2D system for both the cases (α=0, α=1). The jet keeps forming for case γ = 1.25 till $\mu_4$=0.09 while the analytical critical bottom drag value is around 0.0159.

A clearer plot summarizing the runs is shown in Figures 3.17 and 3.18 demarcating the stability boundary, the runs that produced stable jets and the runs that produced no jets. The formula determining the critical Bottom Drag value is given below.

$$\mu_c = \frac{1}{12}(2 - \gamma^2)^2$$

For a given γ any value of bottom drag μ below $\mu_c$ results in the spontaneous evolution of zonal jet.

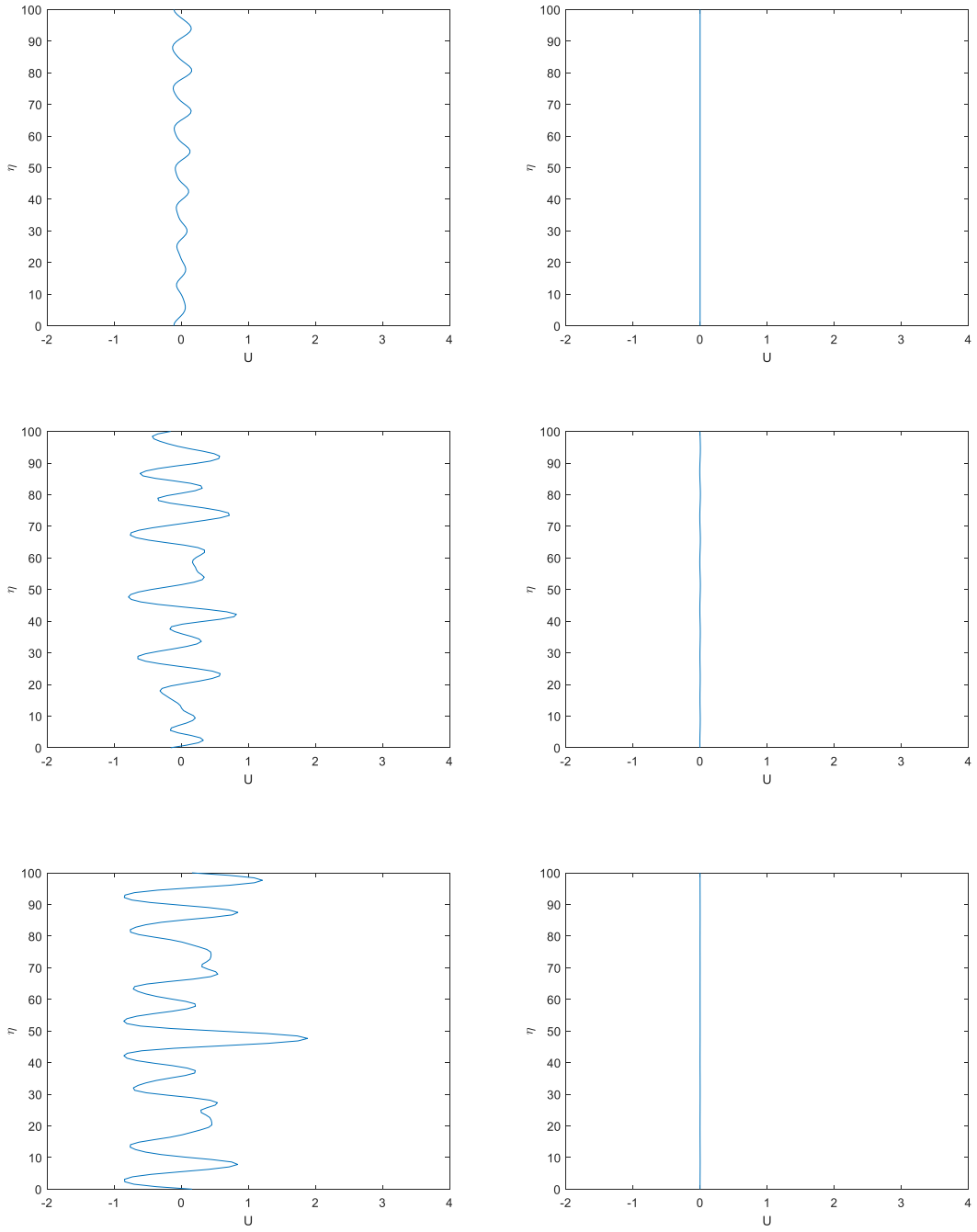


Figure 3.15: Plot Showing the Zonal Mean vs η at the End of τ=2000 for Cases of (γ, μ) = (0.75, 0.175), (0.75, 0.18), (1, 0.075), (1, 0.087), (1.25, 0.016), (1.25, 0.017) for Case α=0 and $\beta_0 = 0.05$

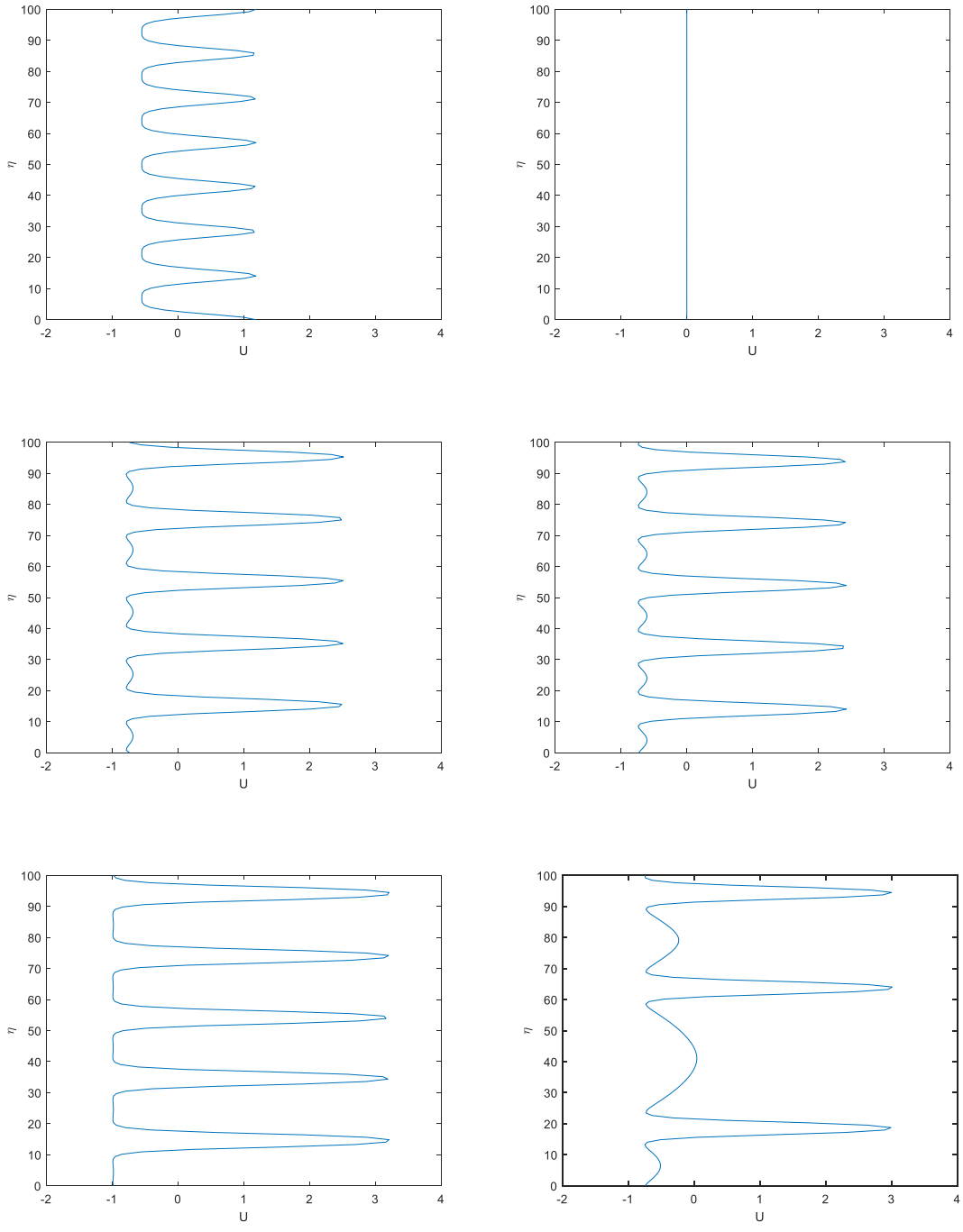


Figure 3.16: Plot Showing the Zonal Mean vs η at the End of τ=2000 for Cases of (γ, μ) = (0.75, 0.175), (0.75, 0.18), (1, 0.086), (1, 0.1), (1.25, 0.017), (1.25, 0.09) for the 1-D System

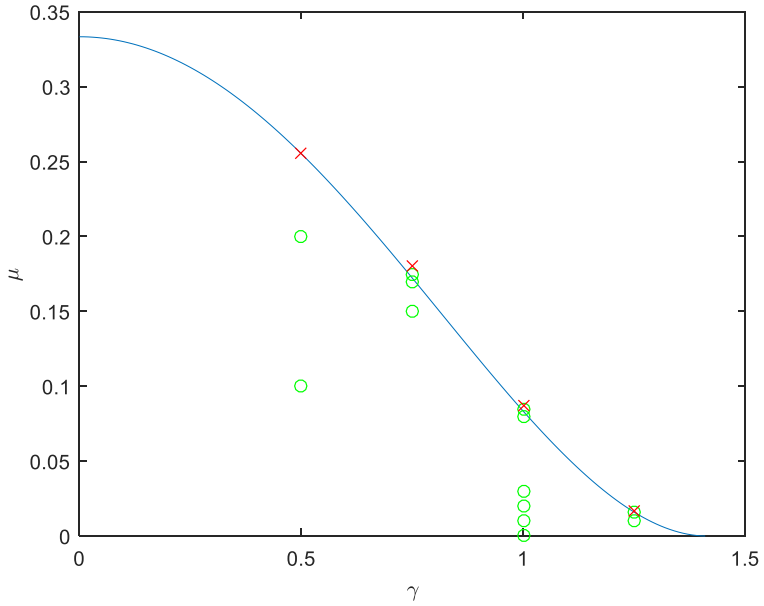


Figure 3.17: Plot Showing the Summary of Runs in the (γ, μ) Parametric Space with Circle Demarcating Formation of Jets while Cross Demarcates Non-Formation of Jets for both the Cases (α=0, α=1)

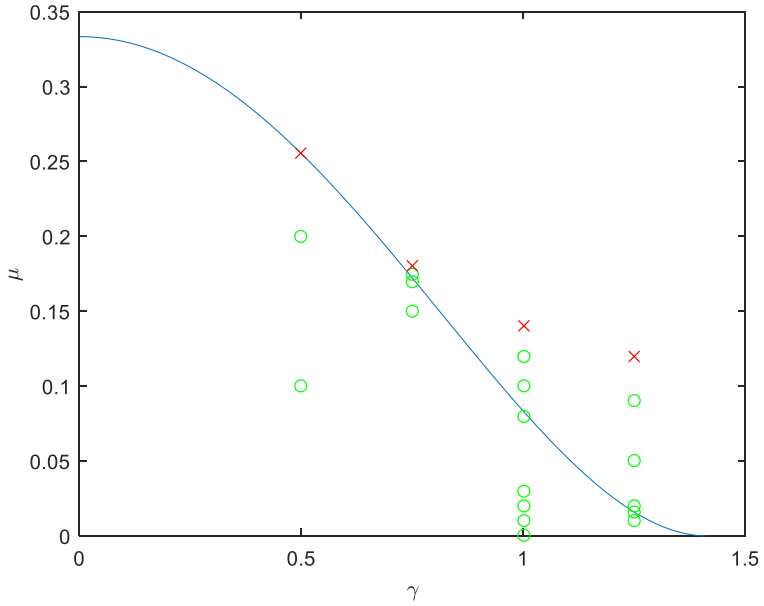


Figure 3.18: Plot Showing the Summary of Runs in the (γ, μ) Parametric Space with Circle Demarcating Formation of Jets while Cross Demarcates Non-Formation of Jets for the 1-D System

3.5 Ratio of Zonal Kinetic Energy to Total Kinetic Energy:

A better understanding of the effect of $\beta_0$ would be to find the ratio of Zonal Kinetic Energy to Total Kinetic Energy. This ratio gives the amount of total energy present in zonal jets. The time evolution of this ratio shown in the figure 3.19 for various $\beta_0$ values provide an illustration on the beginning of formation of Zonal Jets and how the parameter value of $\beta_0$ affects the formation of these Zonal Jets. This Kinetic Energy value is calculated in term of the non-dimensionalized root mean square velocity with Zonal Kinetic Energy considering only the horizontal component of velocity U while Total Kinetic Energy is considered using both the horizontal and vertical component (U & V).

$$U = -A_{\xi}, V = A_{\eta}$$

$$Ratio\ (r) = \frac{KE_{zonal}}{KE_{total}} = \frac{\frac{1}{2}U_{rms}^2}{\frac{1}{2}(U_{rms}^2 + V_{rms}^2)} \qquad (5)$$

This comparison is done for the case of $\alpha$=0. The 1D system is based on the simplification that assumes 100% of the total energy is made up by the zonal jets thus the ratio would be 1 for all the cases. From the plot in Figure 3.19 and 3.20 one clearly see the difference in the rate at which zonal jets are formed for increase in $\beta_0$ value. The initial phase where the ratio keeps increasing indicates the phase where Zonal Jet formation takes place. The later phase when the value remains constants indicates the phase when the upscale energy transfer ceases. We can see that for the case with finite bottom drag ($\mu$=0.01) the halting of upscale energy transfer takes place at a much lesser ratio than that for the case with no bottom drag indicating the persistence of the curvy profile as discussed in section 3.2.3.

Also the plot in figure 3.21 clearly shows this difference in ratio achieved. The slight deviation (at $\mu$=0.01) in the variation of the ratio with bottom drag is due to the formation of eddy like structures in cases of high $\beta_0$ and low $\mu$ as discussed in section 3.2.3.

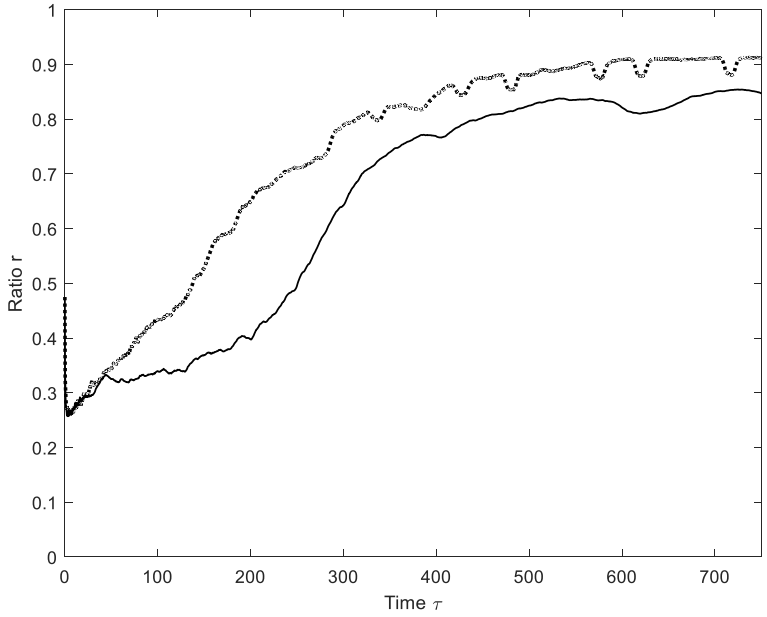


Figure 3.19: Plot Showing the Ratio of Kinetic Energy in Zonal Component to the Total Kinetic Energy for $\mu$=0 with Solid and Dotted Line Representing $\beta_0$=0.01, 0.05 Respectively

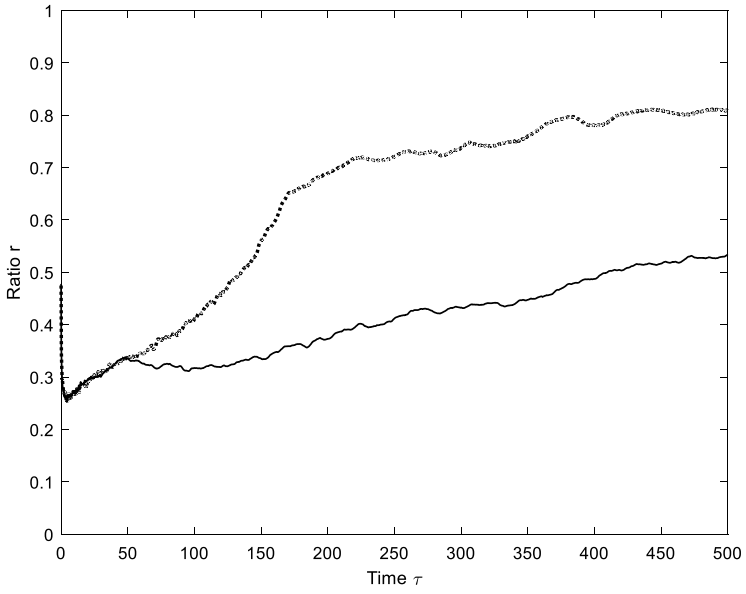


Figure 3.20: Plot Showing the Ratio of Kinetic Energy in Zonal Component to the Total Kinetic Energy for $\mu$=0.01 with Solid and Dotted Line Representing $\beta_0$=0.01, 0.05 Respectively

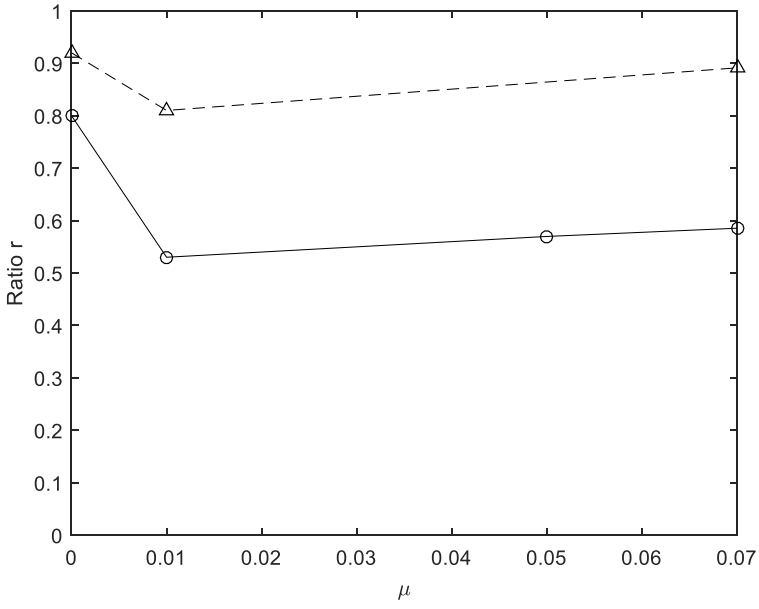


Figure 3.21: Plot Showing the Ratio of Kinetic Energy in Zonal Component to the Total Kinetic Energy for Varying $\mu$ with Solid and Dotted Line Representing $\beta_0$=0.01, 0.05 Respectively at the End of $\tau$=2000.

3.6 Influence of Initial Condition:

It was seen in previous sections that the number of jets and the wavy nature of the jets may have something to do with the initial condition. In order to check the effect of a random and a deterministic initial conditions a simulation was performed for the case with $\beta_0$=0.01 and $\mu$=0.05 with the following initial condition.

$$A\,(\xi, \eta, 0) = \cos(0.12\,\pi\,\xi)\,[1 + sin(0.12\,\pi\,\eta)]$$

The plots for the two cases (with the above initial condition and with random initial condition) are shown in Figure 3.22 and 3.23. It can be seen that despite using a different boundary condition, there is still some wavy nature in the jets though not as much as the case with random boundary condition. This difference in the jet structure is because there is already large scale flow in the initial phase and a bias for zonal jet formation in the form of symmetry in zonal direction.

The figure 3.24 showing the evolution of ratio with time for a case with this initial condition. A striking feature in this plot is the steep reduction in the zonal energy ratio. One can see that after creation of zonally elongated flows a wavy jet is formed which is the reason for the steep fall. Another thing we can see is the number of jets finally formed is the same for this case compared to the case with original random initial condition. This despite the evolution starting with initial six jets. This can be seen in figure 3.25 showing the variation of zonal mean with time.

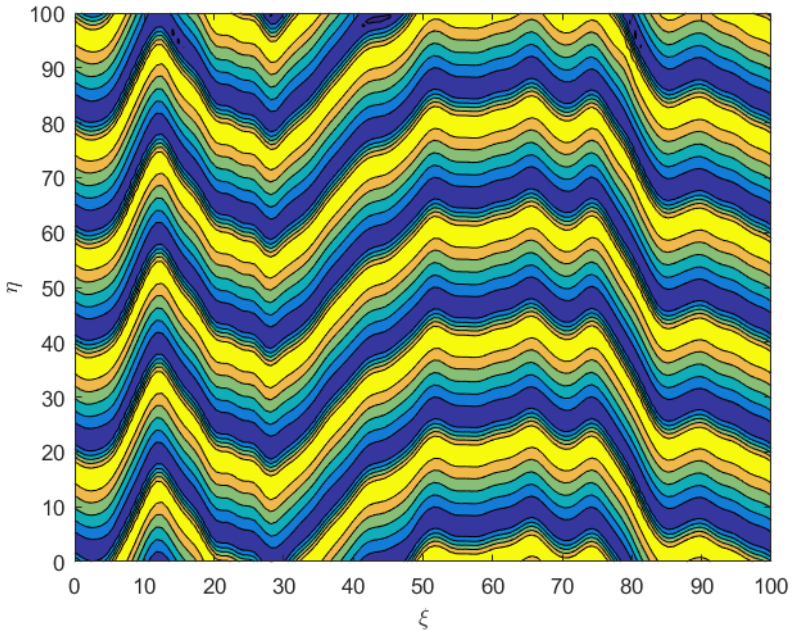


Figure 3.22: Contour Plot of Stream Function for Random Initial Condition Case at $\beta_0$=0.01 and μ=0.05

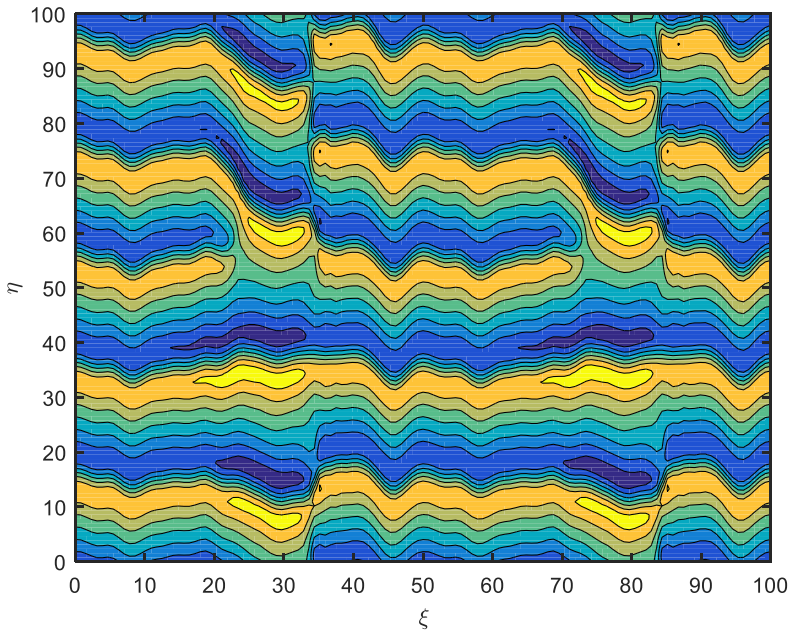


Figure 3.23: Contour Plot of Stream Function for a specific Initial Condition Case at $\beta_0$=0.01 and μ=0.05

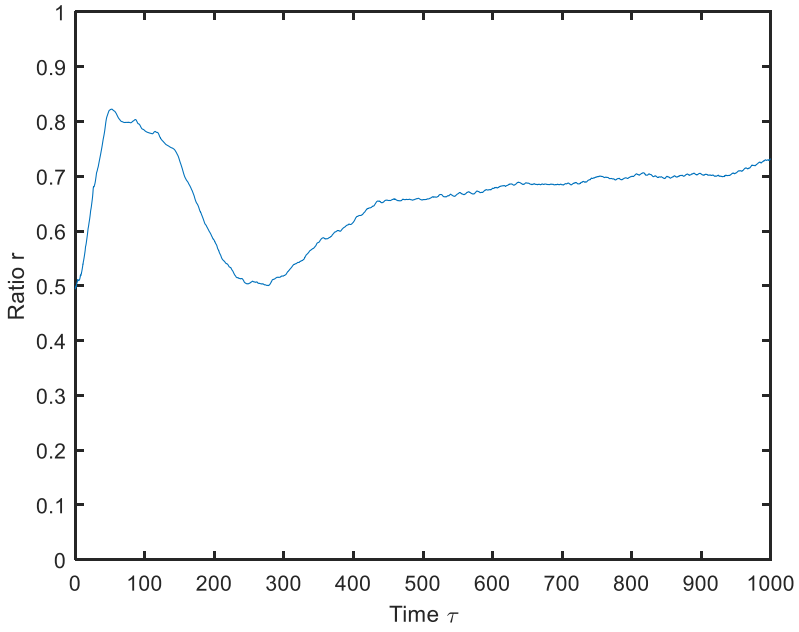


Figure 3.24: Plot Showing the Ratio of Kinetic Energy in Zonal Component to the Total Kinetic Energy for $\beta_0$=0.01 and $\mu$=0.05 for a Specific Initial Condition

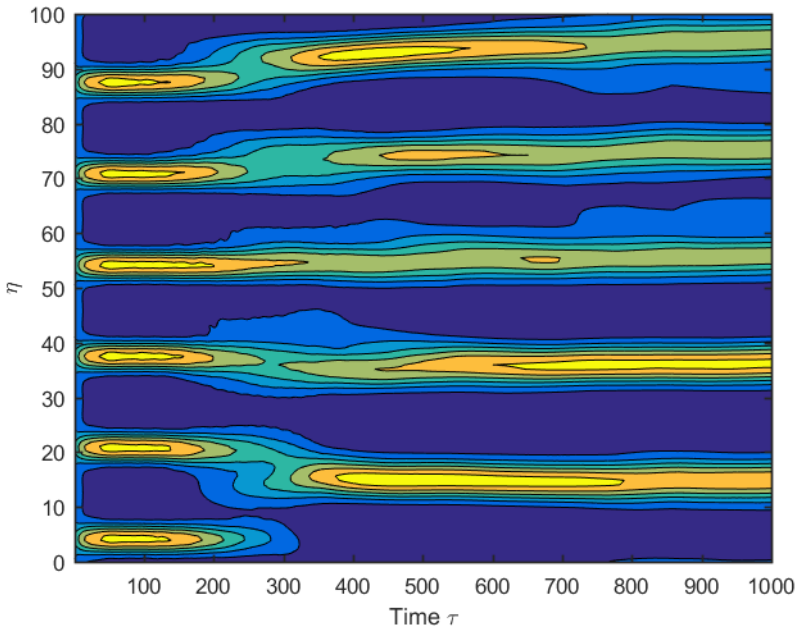


Figure 3.25: Contour Plot of Zonal Mean vs Time for a Specific Initial Condition case at $\beta_0$=0.01 and $\mu$=0.05

3.7 Summary of the Results:

Finally, a plot showing the summary of all the runs is provided in the Figures 3.26 and 3.27 for the 2D system with α=0 and 2D system with α=1. The summary provides the number of jets seen in each of the cases which is given by the number present inside the circular points seen in the results plot.

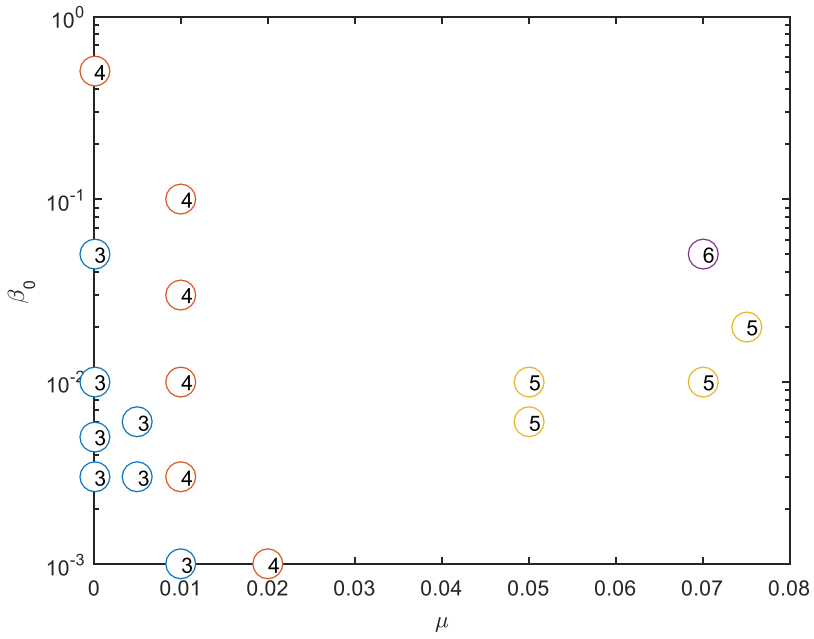


Figure 3.26 Plot Showing the Summary of Runs in the ($\beta_0$, μ) Parametric Space with the Number Inside the Circle Demarcating Number of Jets for α=0 case.

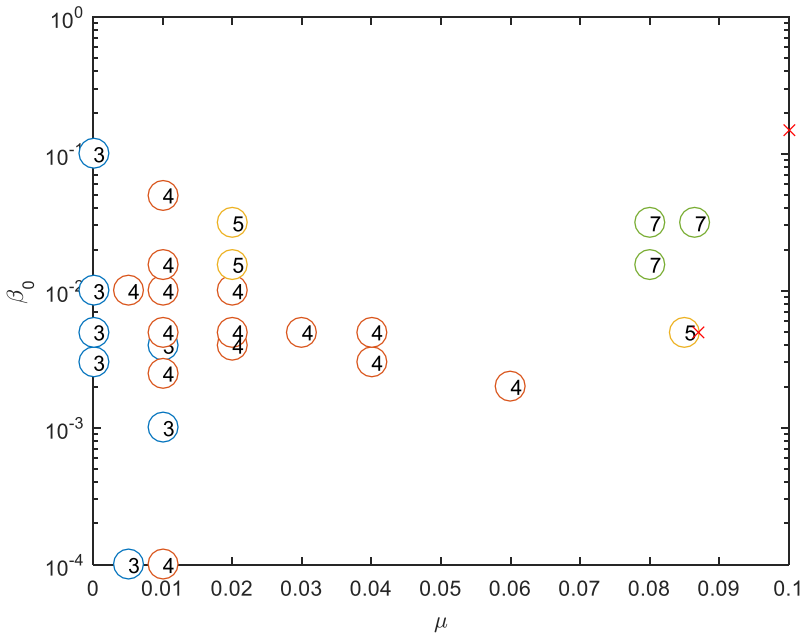


Figure 3.27 Plot Showing the Summary of Runs in the ($\beta_0$, $\mu$) Parametric Space with the Number Inside the Circle Demarcating Number of Jets and Cross Denoting Non-Formation of Jet for $\alpha$=1 Case.

# CHAPTER 4

## 4. CONCLUSION:

Thus, the numerical solutions are explored for the 2-D system spanning the $\beta_0$, $\mu$ parametric space. It is found that certain key behaviors that were predicted from the 1-D system holds true for the 2-D system as well. One is the continuous merger of the zonal jets in the absence of bottom drag which though not conclusive, can still be partially verified from the results. One major result would be the adherence to the $\mu$, $\gamma$ boundary for the formation of jet. It is interesting to note that the boundary that was originally derived analytical from the 1-D system seems to be more suitable for the 2-D system than the original one from which it was derived. On the other hand, there were also certain results that were quite different from behavior suggested by the 1-D system. The formation of wavy jet streams for smaller values of $\beta_0$, and their persistence just like zonal jets is one such phenomena that could not be explained. Similarly, the case of migrating structures in case of an inclined basic state flow was also quite interesting. There is also the presence of large scale long persistent eddies that are seen in the case of large $\beta_0$ and small bottom drag. Another aspect discussed was the variation in the number of jets for varying $\beta_0$ which if not fortuitous due to random initial conditions needs some explanation. The aim of the study was to provide numerical solution to the complete 2-D system investigating in the process any information left out because of its simplification. Despite certain similarities there are certain results which needs future investigation to confirm the veracity of their existence.

# REFERENCES


Berloff. P, Kamenkovich. I and Pedlosky. J, A mechanism of formation of multiple zonal jets in the oceans, J. Fluid Mech. vol. 628, 2009.

Danilov. S and Gryanik V.M, Barotropic Beta-Plane Turbulence in a Regime with Strong Zonal Jets Revisited, Journal of Atmospheric Sciences, 61, 2004.

Gottlieb. S and Chi-Wang Shu, TOTAL VARIATION DIMINISHING RUNGE-KUTTA SCHEMES, Institute for Computer Applications in Science and Engineering, NASA CR-201591, 1996.

Huang, H. P., and Robinson. A, Two-dimensional turbulence and persistent zonal jets in a global barotropic model. J. Atmos. Sci., 55, 611–632, 1998.

Manfroi A. J. and Young W. R., Slow Evolution of Zonal Jets on the Beta Plane, Journal of Atmospheric Sciences, Vol. 56, 1998.

Manfroi A. J. and Young W. R., Stability of β-plane Kolmogorov flow, Physica D 162 (2002) 208–232.

Nakamura Noboru and Zhu Da., Formation of jets through mixing and forcing of potential vorticity: analysis and parameterization of beta-plane turbulence. J. Atmos. Sci., 67, 2010.

Obuse Kiori, Takehiro Shin-ichi, Yamada Michio, Weak interaction between zonal jets on a β plane, Japan J. Indust. Appl. Math. (2013) 30:111–127

Panetta, R. L., Zonal jets in wide baroclinically unstable regions: Persistence and scale selection. J. Atmos. Sci., 50, 2073– 2106, 1993.

Pedlosky J., Geophysical Fluid Dynamics. Springer, 1987.

Rhines, P. B., Waves and turbulence on a beta-plane. J. Fluid Mech., **69,** 1975.

Scott R. K. and Dritschel D. G., The structure of zonal jets in geostrophic turbulence. J. Fluid Mech., 711, 2012.

Vallis G. K. and Mathew E. Maltrud. Generation of mean flows and jets on a beta plane and over topography. Journal of Physical Oceanography, 23, 1992.

Shepherd, T. G., Rossby Wave and two dimensional turbulence in a large scale zonal jet, J. Fluid Mech., 183, 467-509, 1987.

# APPENDIX A

## CODE FOR SOLVING 2-D SYSTEM

```
tic;
clc;
clear;
L=100;
m=128;
h=L/m;
%predeclaration
A=zeros(m+11,m+11);
Ai=zeros(m+11,m+11);
d2a=zeros(m+6,m+6);
U=zeros(m+11,m+11);
Ui=zeros(m+11,m+11);
U_plot=zeros(m+11,m+11);
zonalpoint=zeros(m+11,m+11);
gamma=1;
b0=0.01;
alpha=0;
mu=0.05;
y=0-6*h:h:100+6*h;
x=0-6*h:h:100+6*h;
t=0;
inc=1;
var=1;
```

```
for i=1:length(x)
   for j=1:length(y)
         A(i,j)=cos(1*pi*x(i)/600)*(1+sin(1*pi*y(j)/600));
        %A(i,j)=rand(1);
         Ai(i,j)=A(i,j);
   end
end
figure
surfc(x,y,A);
for rr=1:m
      for ss=1:m
         if rr==ss&&rr~=m
            a(rr,ss)=-2;
         else if rr>=3&&rr-ss==2
               a(rr,ss)=0;
            else if rr>=2&&rr-ss==1
                  a(rr,ss)=1;
               else if ss>=2 && ss-rr==1
                     a(rr,ss)=1;
                  else if ss>=3 && ss-rr==2;
                        a(rr,ss)=0;
                     else if (rr==m-1&&ss==1)||(rr==1&&ss==m-
1)||(rr==m&&ss==2)||(rr==2&&ss==m)
```

```
                    a(rr,ss)=0;
                else if (rr==1&&ss==m)||(rr==m&&ss==1)
                    a(rr,ss)=1;
                else if rr==m&&ss==m
                    a(rr,ss)=1;
                else
                    a(m,rr)=1;
                    a(m,m)=1;
                    a(m,2)=1;
                end
            end
        end
    end
  end
 end
end
   ina=inv(a);
while t<=2
dann=thesfn(A,h,m,gamma,b0,alpha,mu);
for i=7:m+6
```

```
    for j=7:m+6
        d2a(i,j)=(A(i+1,j)-2*A(i,j)+A(i-1,j))/(h^2);
        d4a(i,j)=(A(i+2,j)-4*A(i+1,j)+6*A(i,j)-4*A(i-1,j)+A(i-2,j))/(h^4);
    end
end
dt=min(0.01,0.8*h/(12*gamma*max(max(abs(A)))));
if t<300&&t+dt>300
    dt=300-t;
else if t<500&&t+dt>500
        dt=500-t;
    else if t<600&&t+dt>600
            dt=600-t;
        else if t<1000&&t+dt>1000
                dt=1000-t;
            end
        end
    end
end
%%start of RK-3%%
dann0=dann;
phi0=d2a;
phi1=phi0+dt.*dann0;
A=d2a2a(ina,phi1,h,m);
```

```
A=thesboun(A,m);
dann1=thesfn(A,h,m,gamma,b0,alpha,mu);
phi2=phi1-(3/4)*dt.*dann0+(1/4)*dt.*dann1;
A=d2a2a(ina,phi2,h,m);
A=thesboun(A,m);
dann2=thesfn(A,h,m,gamma,b0,alpha,mu);
phi3=phi2-(1/12)*dt.*dann0-(1/12)*dt.*dann1+(2/3)*dt.*dann2;
A=d2a2a(ina,phi3,h,m);
A=thesboun(A,m);

for i=7:m+7
   for j=7:m+7
      U(i,j)=(A(i-1,j)-A(i+1,j))/(2*h);
      V(i,j)=(A(i,j-1)-A(i,j+1))/(2*h);
      Ued=((abs(U(i,j)))^2+(abs(V(i,j)))^2);
      Uz=((abs(U(i,j)))^2);
      ratio(i,j)=Uz/Ued;
      Ui(i,j)=(Ai(i-1,j)-Ai(i+1,j))/(2*h);
   end
   U_plot(i)=mean(U(i,:));
end
      if rem(inc,100)==0
         t_plot(var)=t;
```

```
            zonalpoint(7:m+7,inc/100)=U(7:m+7,m);
            zonalmean(7:m+7,inc/100)=U_plot(7:m+7);
            contourf(x(7:m+7),y(7:m+7),A(7:m+7,7:m+7));
            F(inc/100)=getframe;
            var=var+1;
        end
rmean(inc)=mean(mean(ratio));
ttot(inc)=t;
contourf(x(7:m+7),y(7:m+7),A(7:m+7,7:m+7));pause (0.000001);
t=t+dt;
inc=inc+1;
end
mov=VideoWriter('b0.01mu0.0862000sa1.avi','Uncompressed AVI');
save('b0.01 mu0a enerrgy ratio.mat');
figure
plot(ttot,rmean);
figure
contourf(t_plot,x(7:m+7),zonalmean(7:m+7,:));
figure
plot(Ui(7:m+7,m),x(7:m+7));xlim([-2 4]);
figure
plot(U_plot(7:m+7),x(7:m+7));
toc;
```

thesfn

```
function [dann] = thesfn(A,h,m,gamma,b0,alpha,mu)
d2a=zeros(m+13,m+13);
d4a=zeros(m+13,m+13);
d6a=zeros(m+13,m+13);
da2=zeros(m+13,m+13);
first=zeros(m+13,m+13);
da3=zeros(m+13,m+13);
dapsi=zeros(m+13,m+13);
da=zeros(m+13,m+13);
term1=zeros(m+13,m+13);
term2=zeros(m+13,m+13);
dann=zeros(m+6,m+6);
for i=4:m+9
   for j=4:m+9
      d2a(i,j)=(A(i+1,j)-2*A(i,j)+A(i-1,j))/(h^2);
      d4a(i,j)=(A(i+2,j)-4*A(i+1,j)+6*A(i,j)-4*A(i-1,j)+A(i-2,j))/(h^4);
      d6a(i,j)=(1*A(i+3,j)-6*A(i+2,j)+15*A(i+1,j)-20*A(i,j)+15*A(i-1,j)-6*A(i-2,j)+A(i-
3,j))/(h^6);
      da2(i,j)=(gamma+((A(i+1,j)-A(i-1,j))/(2*h)))^2;
      first(i,j)=da2(i,j)*(A(i+1,j)-A(i-1,j))/(2*h);
```

```
        da3(i,j)=((A(i+1,j)-A(i-1,j))/(2*h))^3;
        dapsi(i,j)=(A(i,j+1)-A(i,j-1))/(2*h);%h of other coordinate
        da(i,j)=(A(i+1,j)-A(i-1,j))/(2*h);
    end
end
for i=7:m+6
    for j=7:m+6
        term1(i,j)=(-1*first(i-2,j)+2*first(i-1,j)-2*first(i+1,j)+1*first(i+2,j))/(2*(h^3));
        term2(i,j)=(-1*da3(i-2,j)+2*da3(i-1,j)-2*da3(i+1,j)+1*da3(i+2,j))/(2*(h^3));
        dann(i,j)=-2*d4a(i,j)-3*d6a(i,j)+term1(i,j)-(1/3)*term2(i,j)-
b0*dapsi(i,j)+b0*alpha*da(i,j)-mu*d2a(i,j);
    end
end
```

thesbound

```
function [A] = thesboun(A,m)

for j=7:m+6
    A(m+7,j)=A(7,j);
    A(m+8,j)=A(8,j);
    A(m+9,j)=A(9,j);
    A(m+10,j)=A(10,j);
    A(m+11,j)=A(11,j);
```

```
    A(m+12,j)=A(12,j);
    A(m+13,j)=A(13,j);
    A(6,j)=A(m+6,j);
    A(5,j)=A(m+5,j);
    A(4,j)=A(m+4,j);
    A(3,j)=A(m+3,j);
    A(2,j)=A(m+2,j);
    A(1,j)=A(m+1,j);
end
for i=7:m+6
        A(i,m+7)=A(i,7);
    A(i,m+8)=A(i,8);
    A(i,m+9)=A(i,9);
    A(i,m+10)=A(i,10);
    A(i,m+11)=A(i,11);
    A(i,m+12)=A(i,12);
    A(i,m+13)=A(i,13);
    A(i,6)=A(i,m+6);
    A(i,5)=A(i,m+5);
    A(i,4)=A(i,m+4);
    A(i,3)=A(i,m+3);
    A(i,2)=A(i,m+2);
    A(i,1)=A(i,m+1);
```

```
end
for j=1:m+13
    A(1,j)=A(m+1,j);
    A(2,j)=A(m+2,j);
    A(3,j)=A(m+3,j);
    A(4,j)=A(m+4,j);
    A(5,j)=A(m+5,j);
    A(6,j)=A(m+6,j);
    A(m+7,j)=A(7,j);
    A(m+8,j)=A(8,j);
    A(m+9,j)=A(9,j);
    A(m+10,j)=A(10,j);
    A(m+11,j)=A(11,j);
    A(m+12,j)=A(12,j);
    A(m+13,j)=A(13,j);
end
```